Machine learning techniques for investigating the Coulomb friction and hysteresis in structural joints

SAURABH MAHAJAN

Axial load

Push ← → Pull

Outside flange

Inside flange
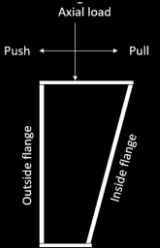
TU Delft

Machine learning techniques for investigating the Coulomb friction and hysteresis in structural joints

by

Saurabh Mahajan

To obtain the degree of Master of Science

at the Delft University of Technology,

to be defended publicly on July 6, 2023 at 9:30 AM.

MSc Thesis

Civil Engineering

Structural Engineering track

Student number: 5464315

Assessment committee

Dr. A. Cicirello (*Chair*)

Dr. F. Kavoura

Dr. E. Lourens

ACKNOWLEDGEMENTS

Abstract

Structural joints influence the design strength, material requirement of a structure. Structural joints experience damping dissipation due to friction damping or hysteresis damping. Damping is often used for reducing the vibrations in a structure. However, large amount of energy dissipation leads to deterioration of the material used for constructing the joint. Hence it is important to identify the system parameters like stiffness, viscous damping, friction force as well as the hysteretic restoring force that cause the energy dissipation in the structure.

For identifying the uncertain system parameters like stiffness, viscous damping and magnitude of friction force, the SINDy algorithm is extended by using stick and slip temporal constraints. This is done by segregating the data of external forcing and response of SDoF system, applying the existing SINDy algorithm and applying the sticking and slipping conditions in the time domain. The proposed Extended SINDy approach estimates the system parameters more accurately compared to the existing SINDy algorithm.

For studying the hysteresis in the structural joints, a pinned column base-plate was considered in an elastic region. Further, the Dahl model with different slope parameter for each branch of moment-rotation hysteresis is employed. The correct values of parameters are estimated using the Bayesian Optimization technique. This procedure yields a functional form representing a resisting hysteretic moment-rotation behaviour in a structural joint with good accuracy.

Contents

List Of Acronyms

ARX   Auto-Regressive with eXogenous input

EOM   Equation Of Motion

ML   Machine Learning

MDoF   Multiple degrees of freedom

NARMAX   Nonlinear Auto-Regressive Moving-Average with eXogenous

NARX   Nonlinear Auto-Regressive with eXogenous

RMSE   Root Mean Squared Error

SDoF   Single Degree of Freedom

SINDy   Sparse Identification of Nonlinear Dynamics

SNR   Signal-to-noise ratio

SR3   Sparse Relaxed Regularized Regression

1. Introduction

1.1. Motivation

A structural joint is a key component in a structural design of a building because the loads are transferred from the beam to columns and from columns to the foundation via a structural joint. A joint can be flexible, semi-rigid, or fully rigid. The rigidity of the structural joints influences the flexibility of a structure and its response to lateral loads. Hence, it is important to study the nonlinear behaviour of a structural joint when subject to different external loading conditions. The nonlinear behaviour of a structural joint is studied by performing computational modelling in finite element softwares as well as using structural health monitoring techniques. Structural health monitoring techniques are widely used for identifying the properties of existing structures using the data of external forcing and the response of the structure to the external forcing. Recently, identifying the properties of an existing structure (nonlinear system identification) using machine learning techniques has acquired the attention of researchers.

The application of the system identification technique depends upon the nonlinearity present in the structure. Some well-known sources of nonlinearities are (i) geometric nonlinearity arising from large displacements of structure [1]; (ii) inertia nonlinearity due to the nonlinear terms of velocities and/ or acceleration [2]; (iii) material nonlinearity caused by the nonlinear stress-strain relationship, e.g. foams [3]; (iv) damping dissipation due to friction effects [4], or hysteric damping [5]. The widely used models for studying damping dissipation are the Dahl model for friction [6] and the Bouc-Wen model [7], [8] for the dynamic systems representing hysteresis.

Friction nonlinearity can be found in Civil Engineering structures such as the grandstands at sporting events [9]. The grandstands are prone to a great amount of nonlinearity, produced by the looseness of joints, which creates friction and unwanted clearance. The friction in the structural joints results in the rise of unwanted vibrations and heat in the structure. As the vibrations are significantly nonlinear, it invalidates the linear-model-based simulation response due to the crowd movement [9]. Hence, it is important to identify the functional

form of the friction force contributing to the dynamic response of engineering systems. This would improve the models employed for predicting the response of structures in operating conditions.

Furthermore, the structural joints are subject to harmonic as well as random dynamic loading because of earthquakes, vibrations due to heavy mechanical machinery. There is a loss of energy (hysteresis) when the column base-plate joint is subjected to a harmonic external excitation as shown in [10]. This is observed via the restoring moment-rotation diagram of the pinned column base-plate connection. The moment-rotation curve of the pinned column base-plate connection shows considerable non-zero rotational stiffness [10]. The accurate prediction of the moment-rotation behaviour will help in the accurate estimation of loss of energy and variation in rotational stiffness. Hence, it is important to study the hysteresis in the pinned column base-plate connection.

1.2. Problem Statement

The scope of this thesis is twofold; firstly, the development of a framework that combines a data-driven system identification technique with stick and slip temporal constraints. This includes identifying governing EOM of the Single Degree of Freedom (SDoF) system subjected to Coulomb friction nonlinearity. This is done by augmenting the existing SINDy algorithm [11] with the stick and slip temporal constraints (Extended SINDy). Later, the robustness of the Extended SINDy algorithm is analyzed under varying noise levels.

Secondly, an equation representing the moment-rotation relationship for a pinned column base-plate connection is proposed. This is achieved by considering the Dahl model with different slope parameter for each branch of hysteresis. Further, the optimum value of slope parameter is estimated using the Bayesian Optimization technique [12]

1.3. Research Question

There are 2 research questions that can be formulated as follows:

1. How to derive the correct Equation Of Motion (EOM) for SDoF dynamic system with the Coulomb friction using a Machine Learning technique with the minimal use of

Introduction

physics?

To successfully answer the first research question, it is further simplified into the following sub-questions:

a) How does the state-of-the-art machine learning algorithm perform, in the case of a discontinuous nonlinearity?

b) What type of data is required as an input for the machine learning algorithm, to correctly identify the governing EOM?

c) Which physics information is missing in the machine learning algorithm and how to incorporate it?

d) How does the proposed machine learning algorithm perform in a noisy environment?

2. How to derive a governing equation representing moment-rotation relationship in a pinned column base-plate connection?

The second research question is further divided into the following sub-questions:

a) How to represent the pinned column base-plate connection schematically?

b) Which pre-existing hysteresis model can reproduce an asymmetric hysteresis similar to the pinned column base-plate connection?

c) How to vary the parameters in the Dahl model to control the shape of hysteresis diagram?

These research questions are answered in this thesis leading:

1. Successful addition of stick and slip temporal constraints to the machine learning algorithm

2. Formulation of strategy to estimate the correct EOM in the presence of discontinuous nonlinearity. This formulation shows good performance for various noise levels

3. Formulation of the governing equation for the pinned column base-plate connection. The estimated equation represents the hysteresis behaviour observed in the moment-rotation diagram when the connection is in the elastic region

1.4. Outline of the thesis

This thesis is composed of 4 chapters. Chapter 2 presents the research paper that discusses the proposed Extended SINDy algorithm for the identification of the dynamic system parameters like stiffness, viscous damping and Coulomb friction (all mass normalized). In Chapter 3, the research paper presents the Dahl model with different slope parameter for each branch of hysteresis for identification of governing equation of pinned column base-plate connection. Chapter 4 reiterates the conclusions drawn in the research papers and discusses the challenges for the current as well as future work.

Bibliography of Chapter 1

[1]   M. Amabili, and M. doussis, "Review of Studies on Geometrically Nonlinear Vibrations and Dynamics of Circular Cylindrical Shells and Panels, with and without Fluid-Structure Interaction", *ASME Appl. Mechanics Review,* vol. 56, pp. 349-381, 2003 https://doi.org/10.1115/1.1565084

[2]   G. Kerschen, K. Worden, A. F. Vakakis, and J. C. Golinval, "Past, Present and Future of Nonlinear System Identification in Structural Dynamics", *Mechanical systems and signal processing*, vol. 20, pp. 505-592, 2006 https://doi.org/10.1016/j.ymssp.2005.04.008

[3]   S. W. White, S. K. Kim, A. K. Bajaj, P. Davies, D. K. Showers, and P. E. Liedtke, "Experimental Techniques and Identification of Nonlinear and Viscoelastic Properties of Flexible Polyurethane Foam", *Nonlinear dynamics*, vol. 22, pp. 281-313, 2000 https://doi.org/10.1023/A:1008302208269

[4]   G. R. Tomlinson, and J. H Hibbert, "Identification of the Dynamic Characteristics of a Structure with Coulomb Friction", *Journal of Sound and Vibration*, vol. 64, pp. 233-242, 1976 https://doi.org/10.1016/0022-460X(79)90648-5

[5]   T.K. Caughey, and A. Vijayaraghavan, "Free and Forced Oscillations of a Dynamic System with Linear Hysteretic Viscous damping", *International Journal of Non-Linear Mechanics,* vol. 5, pp. 533-555, 1970 https://doi.org/10.1016/0020-7462(70)90015-6

[6]   P. R. Dahl, "A Solid Friction Model", Aerospace Corp El Segundo, 1968

[7]   R. Bouc, "Forced Vibrations of Mechanical Systems with Hysteresis", *Proc. of the Fourth Conference on Nonlinear Oscillations,* 1967

[8]   Y. K. Wen, "Method for Random Vibration of Hysteretic Systems", *Journal of the engineering mechanics division*, vol. 102, pp. 249-263, 1976 https://doi.org/10.1061/JMCEA3.0002106

[9]   K. Worden, G. R. Tomlinson, "Nonlinearity in Structural Dynamics", 2001 https://doi.org/10.1201/9780429138331

[10]   F. Kavoura, B. Gencturk, and M. Dawood, "Reversed Cyclic Behavior of Column-to-Foundation Connections in Low-Rise Metal Buildings", *Journal of Structural*

Bibliography of Chapter 1

Engineering, vol. 143, 2017 https://doi.org/10.1061/(ASCE)ST.1943-541X.0001821

[11]   S. L. Brunton, J. L Proctor, and J. N. Kutz, "Discovering Governing Equations from Data by Sparse Identification of Nonlinear Dynamical Systems", *Proceedings of the national academy of sciences,* vol. 113, pp. 3932-3937, 2016 https://doi.org/10.1073/pnas.151738411

[12]   M. Pelikan, D. E. Goldberg, and E. Cantú-Paz, "Boa: The Bayesian Optimization Algorithm", *Proceedings of the genetic and evolutionary computation*, vol. 1, pp 525-32, 1999

List Of Figures In Chapter 2

List Of Tables In Chapter 2

2. Research Paper 1

Governing equation identification of nonlinear single degree of freedom oscillators with Coulomb friction using explicit stick and slip temporal constraints

Saurabh Mahajan[1], Alice Cicirello[1]

[1] Faculty of Civil Engineering and Geosciences

Delft University of Technology,

Delft, 2628 CN, South Holland, The Netherlands.

Abstract

The friction force at joints of engineering structures is usually unknown and not directly identifiable. This contribution explores a procedure for obtaining the governing equation of motion and correctly identifying the unknown Coulomb friction force of a mass-spring-dashpot system. In particular, a Single-Degree-of-Freedom system is investigated both numerically and experimentally. The proposed procedure extends the state-of-the-art data-driven SINDy algorithm by developing a methodology that explicitly imposes constraints encoding knowledge of the non-smooth dynamics experienced during stick-slip phenomena. The proposed algorithm consists of three steps: (i) data segregation of mass-motion from mass-sticking during stick-slip response; (ii) application of SINDy on the mass-motion dataset to obtain the functional form of the governing equation; (iii) applying sticking and slipping conditions to identify the unknown system parameters. It is shown that the proposed approach yields an improved estimate of the uncertain system parameters such as stiffness, viscous damping, and magnitude of friction force (all mass normalized) for various signal-to-noise ratios compared to SINDy.

Keywords: Stick and slip temporal constraints, Nonlinear dynamic system identification, SINDy, Epistemic uncertainty, Discontinuous nonlinearity, Coulomb friction

2.1. Introduction

The dynamics of various engineering structures like wind turbines, robots, buildings, etc. are greatly influenced by the friction present in joints. The amplitude of structural response can be drastically reduced due to the loss of energy resulting from frictional contact. As a result of heat produced because of friction, repetitive motion can cause wear and tear of the surfaces in contact with each other. Hence, it is important to identify the functional form of the friction force contributing to the dynamic behaviour of engineering systems as it would improve models employed for predicting the response of structures in operating conditions. Currently, it is not possible to directly characterise the friction force of structural joints without affecting the joint behaviour itself. Consequently, the friction force can be regarded as an epistemic uncertainty, that is uncertainty caused by lack of knowledge. To this end, a large body of research has focused on the use and development of system identification approaches which use measurements of output and input signals to a dynamic system. These approaches can be broadly grouped into: (i) approaches based on an equivalent linearization techniques as well as stochastic linearization methods [1-5]; (ii) time-domain methods, such as Auto-Regressive with eXogenous input model (ARX) for linear systems [1], [6], [7] and Nonlinear Auto-Regressive with eXogenous (NARX), Nonlinear Auto-Regressive Moving-Average with eXogenous inputs model (NARMAX) for nonlinear system identification [8]. However, the NARX model fails to capture the noise as a separate entity which is overcome by NARMAX. However, NARMAX models the nonlinearity as a polynomial function which might limit its applicability; (iii) approaches leveraging on Machine Learning strategies because of the availability of measurement on the external excitation and response of nonlinear systems. The last group has recently gained particular interest in the research community [9]. The Sparse Identification of Nonlinear Dynamics (SINDy) [10], [11], [12] belongs to this group and has recently been applied to estimate the governing Equation Of Motion (EOM) based on the data of input and output of a dynamic system. SINDy has been applied for identifying EOM in the chemical reactor [13], parameters of the power grid model [14], and delayed differential equation [15]. In particular, in nonlinear structural dynamics, it has been used for estimating nonlinear normal modes [16], and reconstructing governing EOM for geometrical nonlinear systems

[17]. However, in the presence of a discontinuous nonlinearity, e.g., frictional joints subject to the stick-slip motion, the error in predictions of the SINDy algorithm can be substantial, as shown in this paper. This leads to errors in the estimates of the epistemic uncertain system parameters such as stiffness, viscous damping and value of nonlinear force in a dynamic system (all mass normalized), which are fixed but unknown.

To address this issue for a Single Degree of Freedom (SDoF) system with Coulomb friction subject to a harmonic excitation, the Extended SINDy is proposed by introducing two key modifications to SINDy [10]. Firstly, in the stick-slip dynamic regime, the data of response and forcing is segregated into mass-sticking and mass-motion. Further the data of mass-motion is used as an input for the existing SINDy algorithm to identify the correct functional form of EOM. Secondly, the correct functional form of the EOM is used to enforce the physics-based constraints to estimate the epistemic uncertain system parameters. The applicability and accuracy of the Extended SINDy algorithm for obtaining the EOM are explored and compared to SINDy, also in the presence of varying noise levels.

2.2. Sparse Identification of Nonlinear Dynamics (SINDy) Algorithm: Review and applicability

2.2.1. Review

Let us consider a dynamic system whose governing equations can be written as [10]

$$\frac{d}{dt}\boldsymbol{x}(t) = \boldsymbol{f}(\boldsymbol{x}(t)) \qquad \text{Eq. (1)}$$

Where $\boldsymbol{x}(t)$ is the state vector with n number of states of the system at general time instant t ($\boldsymbol{x}(t) = [x_1(t), x_2(t), \dots, x_n(t)]^T$) and $\boldsymbol{f}(\boldsymbol{x}(t))$ is a vector that represents the dynamic system in terms of mass, stiffness, viscous damping and nonlinear forces present in the system. By explicitly accounting for an external forcing $\boldsymbol{u}(t)$, Eq. (1) can be rewritten as [10]

$$\frac{d}{dt}\boldsymbol{x}(t) = \boldsymbol{f}(\boldsymbol{x}(t), \boldsymbol{u}(t)) \qquad \text{Eq. (2)}$$

The system's response ($\boldsymbol{X}$) to the forcing ($\boldsymbol{U}$) can be written in a matrix form to account for the N discrete time steps as [10]

$$X = \begin{bmatrix} x^T(t_1) \\ x^T(t_2) \\ \vdots \\ \cdot \\ \cdot \\ x^T(t_N) \end{bmatrix} = \begin{bmatrix} x_1(t_1) & x_2(t_1) & \cdots & x_n(t_1) \\ x_1(t_2) & x_2(t_2) & \cdots & x_n(t_2) \\ \vdots & \vdots & \ddots & \vdots \\ x_1(t_N) & x_2(t_N) & \cdots & x_n(t_N) \end{bmatrix} \qquad \text{Eq. (3)}$$

$$U = \begin{bmatrix} u^T(t_1) \\ u^T(t_2) \\ \vdots \\ \cdot \\ \cdot \\ u^T(t_N) \end{bmatrix} = \begin{bmatrix} u_1(t_1) & u_2(t_1) & \cdots & u_n(t_1) \\ u_1(t_2) & u_2(t_2) & \cdots & u_n(t_2) \\ \vdots & \vdots & \ddots & \vdots \\ u_1(t_N) & u_2(t_N) & \cdots & u_n(t_N) \end{bmatrix} \qquad \text{Eq. (4)}$$

$$\dot{X} = \begin{bmatrix} \dot{x}^T(t_1) \\ \dot{x}^T(t_2) \\ \vdots \\ \cdot \\ \cdot \\ \dot{x}^T(t_N) \end{bmatrix} = \begin{bmatrix} \dot{x}_1(t_1) & \dot{x}_2(t_1) & \cdots & \dot{x}_n(t_1) \\ \dot{x}_1(t_2) & \dot{x}_2(t_2) & \cdots & \dot{x}_n(t_2) \\ \vdots & \vdots & \ddots & \vdots \\ \dot{x}_1(t_N) & \dot{x}_2(t_N) & \cdots & \dot{x}_n(t_N) \end{bmatrix} \qquad \text{Eq. (5)}$$

Hence the final form of the governing equation of dynamic system is written in a standard state-space formulation as [18]

$$\dot{X} = AX + BU \qquad \text{Eq. (6)}$$

Where A and B are the state and input matrix, respectively. SINDy [10] identifies the unknown governing EOM from the available data of external forcing and of the response to external forcing. The identification is performed using sparsity promoting techniques and machine learning. Some user-specified set of functions which might be contributing to describe the governing EOM of the dynamic system are listed (e.g. see Eq. (7)). A sparse regression with low risk of overfitting is obtained by the combination of sparsity and user-specified terms, producing a parsimonious model [10]. The user-specified terms are included in the candidate function library $\Theta(X)$ which might contain polynomial terms, trigonometric terms, exponential terms and other user-specified functions (e.g. g(**X**)), or their combination [10]. For example:

$$\Theta(X) = \begin{bmatrix} I & X & X^{P2} & X^{P3} & \ldots & sin(X) & cos(X) & e^X g(X) .. \end{bmatrix} \qquad \text{Eq. (7)}$$

Where the $N \times n$ matrix representing i^{th} order polynomial terms is

$$X^{Pi} = \begin{bmatrix} x_1^{i}(t_1) & x_2^{i}(t_1) & \cdots & x_n^{i}(t_1) \\ x_1^{i}(t_2) & x_2^{i}(t_2) & \cdots & x_n^{i}(t_2) \\ \vdots & \vdots & \ddots & \vdots \\ x_1^{i}(t_N) & x_2^{i}(t_N) & \cdots & x_n^{i}(t_N) \end{bmatrix} \qquad \text{Eq. (8)}$$

A selection matrix $\Xi = [\xi_1 \xi_2 \, \xi_3 \, .. \, \xi_n]$ is then introduced, such that the final equation in the state-space form is written as [10]

$$\dot{X} = \Theta(X)\Xi \qquad \text{Eq. (9)}$$

The selection matrix Ξ selects the terms in Eq. (7) that will be present in the governing EOM [10]. This is done by introducing an optimizer with specific minimization function [10]. For example, if the Sequential Threshold Least Squares (STLSq) is used, the minimization function is given by [10]

$$\left\| \dot{X} - \Theta(X)\Xi \right\|_2^2 + \alpha \|\Xi\|_2^2 \qquad \text{Eq. (10)}$$

Where, α is a coefficient that is chosen by the user to boost the sparsity of the terms in the governing EOM. A high value of α leads to a smaller number of terms in the governing EOM.

2.2.2. Applicability of SINDy to friction problems

Although never explicitly mentioned in the literature, the applicability of the SINDy algorithm [10] depends on the functional form of the governing EOM. The dynamic system might contain a nonlinear restoring force term which is discontinuous or changes abruptly in the time domain leading to a non-smooth response. The non-smooth response is a response where the dynamic system changes abruptly from one motion regime to another in the time domain. For example, when the restoring force is a function of signum as in the case of the Coulomb friction model, the response of a SDoF dynamic system with such friction model can be characterized by a sequence of mass-motion and mass-sticking regimes. The EOM representing such a dynamic system is stiff [19]. Without any specified constraints, SINDy performs a regression poorly on such a sequence of regimes to estimate an EOM that would fit simultaneously both mass-motion and mass-sticking. As a major part of the regime consists of mass-motion, the SINDy algorithm would identify the correct functional form of the EOM. However, the coefficients of the identified EOM would be inaccurate.

Let us consider a SDoF dynamic system with friction subject to a harmonic excitation $u(t) = A \sin(\omega t)$ (where A and ω denote the amplitude and frequency of harmonic base excitation respectively), as shown in Fig. 1 (a), and described by:

$$m\ddot{x}(t) + c\dot{x}(t) + kx(t) + F_f sgn[\dot{x}(t)] = ku(t) + c\dot{u}(t) \qquad \text{Eq. (11)}$$

Where, k, c, m, F_f, $x(t)$ and $u(t)$ are the stiffness, viscous damping, mass, friction force magnitude, displacement of SDoF, and harmonic base excitation, respectively, all represented in SI units. The magnitude of friction force (F_f) is defined as a product of the coefficient of friction (μ) and the normal force exerted by mass on the surface. The function sgn[.] represents signum function.

Table 1 Properties of synthetic as well as experimental dynamic system

Quantity	Description	Value	Units
$\hat{k}$	Mass normalized stiffness	358.706	$\dfrac{N}{m.kg}$
$\hat{c}$	Mass normalized viscous damping	0.0658	$\dfrac{Ns}{m.kg}$
$\widehat{F}_f$	Mass normalized magnitude of friction force	0.0856	$\dfrac{N}{kg}$

The EOM of such a system can be represented in a state-space form as

$$\begin{cases} x_1(t) = x(t) \\ \begin{bmatrix} \dot{x}_1(t) \\ \dot{x}_2(t) \end{bmatrix} = \begin{bmatrix} 0 & 1 \\ -\hat{k} & -\hat{c} \end{bmatrix} \begin{bmatrix} x_1(t) \\ x_2(t) \end{bmatrix} + \begin{bmatrix} 0 \\ -\widehat{F}_f \operatorname{sgn}[\dot{x}(t)] \end{bmatrix} + \begin{bmatrix} 0 \\ \hat{k}u(t) + \hat{c}\dot{u}(t) \end{bmatrix} \forall x_2 \neq 0 \end{cases} \quad \text{Eq. (12)}$$

Where, $\hat{k}$, $\hat{c}$, $\widehat{F}_f$, $x_2(t)$ are the mass-normalized stiffness, viscous damping, friction force magnitude, velocity of SDoF, respectively (see Table 1). It is worth mentioning that the synthetic data is obtained by numerically solving Eq. (12) with *ode45* function in MATLAB [20] and explicitly setting the event conditions as explained in [19] for dealing with stiff problems. The event conditions are [21]

$$\left| \hat{c}\dot{u}(t) + \hat{k}u(t) - \hat{k}x_1(t) \right| \leq \widehat{F}_f \boldsymbol{I} \quad \text{Eq. (13)}$$

$$\left| \hat{c}\dot{u}(t) + \hat{k}u(t) - \hat{k}x_1(t) - \dot{x}_2(t) - \hat{c}x_2(t) \right| \geq \widehat{F}_f \boldsymbol{I} \quad \text{Eq. (14)}$$

Where $|.|$ denotes absolute value, $\boldsymbol{t}$ is a vector representing different time instants $\boldsymbol{t} = [t_1 \quad t_2 \quad \cdots \quad t_N]^T$ and $\boldsymbol{I}$ denotes a vector with all entries as 1, respectively.
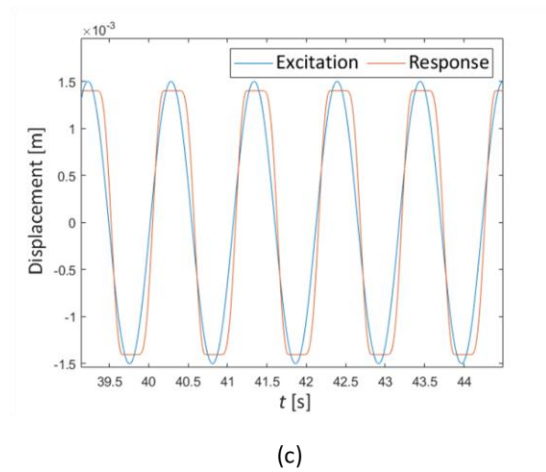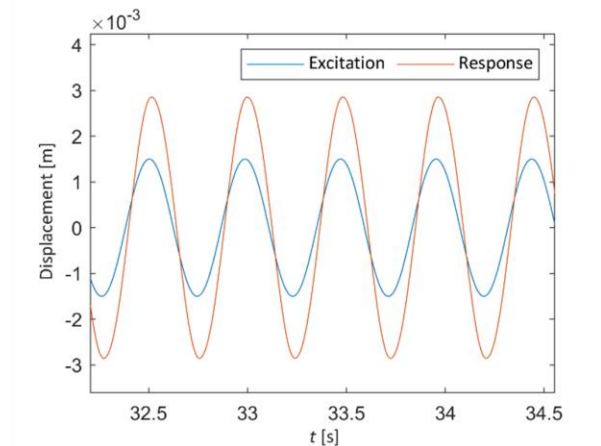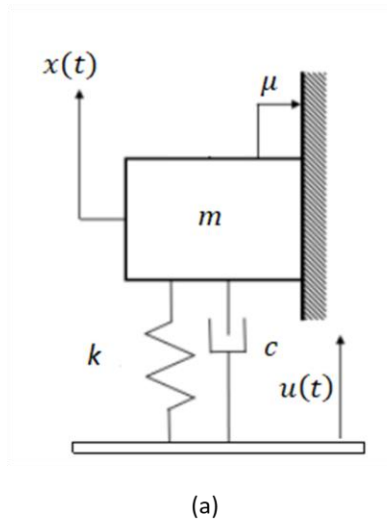
Fig. 1 Schematic representation of SDoF with friction (a), response of SDoF in continuous motion (b) and stick-slip motion (c)

The physical meaning of Eq. (13) is that the mass will indefinitely remain still until Eq. (13) is satisfied [21]. Further, the mass will remain in motion until Eq. (14) is satisfied. This can be further interpreted as follows [21]: when the velocity is zero and the mass is sticking, the friction force is sufficient to resist the inertial force, spring force, and viscous damping force – as described by Eq. (13); when the velocity is non-zero, the friction force is insufficient to resist the restoring forces as described by Eq. (14). This mass-sticking and mass-motion phenomenon cannot be accurately represented by solving Eq. (12) numerically. Hence, the event conditions are explicitly enforced.

Further, $x_1(t)$ and $x_2(t)$ represent the displacement and velocity of SDoF dynamic system in continuous time domain. To perform the analysis in discrete time domain, the

Research Paper 1

displacement and velocity are represented as vectors $x_1(t)$ and $x_2(t)$. $\dot{x}_2(t)$ is obtained by numerically differentiating $x_2(t)$. In this paper, the smooth finite differentiation available in PySINDy package is used for performing the numerical differentiation. In particular, the Savitzky-Golay filter is used in smooth finite differentiation. The window length specified in smooth finite differentiation governs the accuracy of the differentiation. The base is excited at different excitation frequencies (see Table 2) to investigate the response of the mass in continuous, 2-stop stick-slip, and 4-stop stick-slip regime. The continuous and the stick-slip motion of the SDoF system shown in Fig. 1 (b) and Fig. 1 (c) are obtained for the values of system parameters specified in Table 1.

Table 2 Base excitation frequencies for synthetic and experimental case study

	Base excitation frequencies (Hz)		
	Continuous motion	2-stop stick-slip motion	4-stop stick-slip motion
Synthetic case study	2.013, 2.583, 4.611	0.95, 1.034, 1.11	0.47, 0.51, 0.54
Experimental case study	2.013, 2.583, 4.611	1.023, 1.07, 1.10	0.61, 0.62, 0.64

From external excitation and response data, the SINDy [10] is applied to estimate the governing EOM in state-space form. The nonlinear system identification is done in the Python package for SINDy (PySINDy) [11]. PySINDy includes a candidate library and an optimizer for performing regression analysis on the collected data. The custom library chosen for the problem at hand includes linear polynomials and signum functions. For regression analysis, the Sequential Threshold Least Squares (STLSq) and Sparse Relaxed Regularized Regression (SR3) [22] optimizer are selected for continuous and stick-slip motion, respectively. The threshold values of 0.01 and 0.05 are used for STLSq and SR3 respectively. SR3 optimizer is used with the constraint $\frac{dx_1(t)}{dt} = x_2(t)$. Further, the SINDy is used to obtain the governing EOM as shown in Table 3.

As anticipated, it is observed from Fig. 2 that the SINDy algorithm estimates the governing EOM with good accuracy in the case of continuous motion. However, from Table

16

3, it is observed that SINDy [10] fails to identify the coefficients of the EOM correctly in the case of 2-stop and 4-stop stick-slip motion. Based on this physics understanding of the problem, it is clear that there is a need to incorporate explicitly the stick and slip temporal constraints stated in Eq. (13) and Eq. (14).

2.3. Extended SINDy

The Extended SINDy is an approach proposed to address the identification of the governing equation of the SDoF system with Coulomb friction, and it is generally applicable to the dynamic system with discontinuous restoring force when the physics constraints in the time domain are known along with the measurements of the input and output of such system. The main idea behind the Extended SINDy is to augment the pre-existing SINDy algorithm by explicitly enforcing the physics constraints in the time domain by means of a three-step procedure. The detailed step-by-step procedure is described in the following subsections.

2.3.1. Step 1: Data segregation

Consider a SDoF system with Coulomb friction system subject to a harmonic excitation described by Eq. (12). In the stick-slip regime, the motion is a combination of mass-motion and mass-sticking. To obtain a correct functional form of the EOM, the data points of mass-motion and mass-sticking are stored separately. The segregation is done based on the condition applied to the velocity at each time instant as

$$\begin{cases} |x_2(t)| \leq v_{stop} \rightarrow t\epsilon t_{stop} \rightarrow x_{stop} = x(t_{stop}) \\ |x_2(t)| > v_{slip} \rightarrow t\epsilon t_{slip} \rightarrow x_{slip} = x(t_{slip}) \end{cases} \qquad \text{Eq. (15)}$$

Where v_{stop} and v_{slip} denote the cut-off velocity for mass-stop and mass-motion respectively. These values are specified by the user and are based on the available measurements of the velocity. The v_{stop} will strongly depend on the noise level in the measurements and will be chosen such that $v_{stop} \sim 0$. As a rule of thumb, v_{slip} is chosen such that $v_{slip} \gg v_{stop}$ and $v_{slip} \approx \max\left(\frac{|x_2(t)|}{20}\right)$.

2.3.2. Step 2: Using PySINDy

The data points of mass-motion are used as an input to the SINDy [10] algorithm implemented in PySINDy [11], and the functional form of the EOM is identified. The steps within SINDy have been already described in section 2.2.1. The computational cost of this step is equivalent to that of using SINDy. By implementing the STLSq and SR3 the number of iterations needed to converge to a sparse solution is drastically reduced when compared to the LASSO [10].

2.3.3. Step 3: Adding constraints on mass-sticking and mass-motion datasets

In this step, both mass-sticking data and mass-motion data are used. The optimization constraint in Eq. (13) is applied to the former, while the Eq. (14) is applied to the latter. As the physics-based constraints are added in the time domain, this approach is different from the pre-existing approach of applying constraints using an SR3 optimizer [22]. SR3 optimizer requires the user to specify the dependency of each coefficient appearing in the governing EOM.

While Eq. (13) yields the lower bound limit of $\hat{k}$, $\hat{c}$, $\widehat{F}_f$; hence, the region above the lower bound surface is the solution, Eq. (14) provides the upper bound limit and thus the region below the upper bound surface is the solution. The lower bound and the upper bound surfaces are calculated as follows. By indicating with $(t_{stop})_j$ and $(t_{slip})_l$ the jth and l^{th} time instants for mass-sticking and mass-motion, respectively, the lower bound $\Phi_1(\hat{k}, \hat{c})$ is obtained by using the mass-sticking condition in

$$\begin{cases} \left| \hat{c}\dot{u}(t_{stop})_j + \hat{k}u(t_{stop})_j - \hat{k}x_1(t_{stop})_j \right| = \widehat{F}_{f_j} \\ \phi_j(\hat{k}, \hat{c}) = \widehat{F}_{f_j}(\hat{k}, \hat{c}) \\ \Phi_1(\hat{k}, \hat{c}) = max \left| \phi_j(\hat{k}, \hat{c}) \right| \end{cases} \qquad \text{Eq. (16)}$$

And the upper bound $\Phi_2(\hat{k}, \hat{c})$ surfaces is obtained by using the mass-motion condition

$$\begin{cases} \left| \hat{c}\dot{u}(t_{slip})_l + \hat{k}u(t_{slip})_l - \hat{k}x_1(t_{slip})_l - \dot{x}_2(t_{slip})_l - \hat{c}x_2(t_{slip})_l \right| = \widehat{F}_{f_l} \\ \phi_l(\hat{k}, \hat{c}) = \widehat{F}_{f_l}(\hat{k}, \hat{c}) \\ \Phi_2(\hat{k}, \hat{c}) = min \left| \phi_l(\hat{k}, \hat{c}) \right| \end{cases} \qquad \text{Eq. (17)}$$

Where, $\widehat{F}_{f_j}$ and $\widehat{F}_{f_l}$ are the lower bound and upper bound values of friction at j^{th} and l^{th} time instant respectively. As a result, the terms $\hat{k}$, $\hat{c}$, $\widehat{F}_f$ which uniquely identify the system in

Eq. (16) and Eq. (17) are not known. As both the lower bound and an upper bound represent the same dynamic system, intuitively, there should be only one triplet of $\hat{k}$, $\hat{c}$, $\hat{F}_f$, that satisfies both surfaces. However, the generation of both surfaces is affected by numerical errors due to numerical differentiation of the measurements of position and velocity of the mass and of the input. Hence, rather than estimating the $\hat{k}$, $\hat{c}$ optimum point, it is proposed to evaluate the distance D between two surfaces perpendicular to the $\hat{k}\hat{c} -$ plane defined as

$$D(\hat{k}, \hat{c}) = |\Phi_2(\hat{k}, \hat{c}) - \Phi_1(\hat{k}, \hat{c})|$$ Eq. (18)

Where, the distance (D) is the function of mass normalized stiffness and mass normalized viscous damping. Furthermore, the optimum triplet $\left(\hat{k}_*, \hat{c}_*, \hat{F}_{f_*}\right)$ is chosen where $D(\hat{k}, \hat{c})$ is minimum and hence the problem is defined as

$$(\hat{k}_*, \hat{c}_*) = \underset{\hat{k}, \hat{c}}{argmin}[D(\hat{k}, \hat{c})]$$ Eq. (19)

$$\hat{F}_{f_*} = \Phi_1(\hat{k}_*, \hat{c}_*)$$ Eq. (20)

The optimum system parameters are then updated in the EOM found in step 2 of the Extended SINDy. The accuracy of the identification of the optimum parameters is dependent on the noise levels in the measurement, and the window length selected to carry out the numerical differentiation of the input and output measurements. The accuracy of the numerical differentiation is also dependent on the presence of abrupt changes in the time domain caused by the non-smooth response due to stick-slip phenomena. In particular, it is expected to observe an accuracy reduction as the number of stops per cycle in the stick-slip motion increases. All of the above will affect the generation of the upper bound and lower bound surfaces, and consequently the identification error on each term of the EOM. The computational cost of this step is negligible, since it requires evaluating over a grid of k,c parameters the values of friction force according to Eq. (13) and Eq. (14), rather than carrying out the full nonlinear analyses for each grid point. This means that the optimization in Eq. (19) is carried out explicitly having evaluated the objective function at every point of the grid. This proposed methodology is applied to the stick-slip motion with 2-stops as well as 4-stops.

2.4. Synthetic Model Case Study

Consider a SDoF oscillator with Coulomb friction contact subject to a harmonic excitation as represented in Eq. (11) and Fig. 1. The physical properties of the system are stated in Table 1. The base is excited at different frequencies to obtain continuous as well as stick-slip motion. These frequencies are mentioned in Table 2. The amplitude of base excitation is 0.0015 m. The synthetic data is generated by solving Eq. (11) with *ode45* in MATLAB [20] with explicit event conditions. Both input and output datasets are then used to investigate the identification of the system parameters $(\hat{k}_*, \hat{c}_*, \hat{F}_{f_*})$ and the governing EOM with the Extended SINDy. The hyperparameters used for the Extended SINDy are specified in Table 4.

The results obtained by using Extended SINDy for various noise levels are then compared in terms of Root Mean Square Error (RMSE) and in terms of the relative percentage error in the estimate of the coefficients of the governing EOM to those yielded by SINDy and to their true values (as specified in Table 1) Indicating with $x_1(t)$ the synthetic data, with $[x_1(t)]_*$ the solution of the governing EOM obtained with SINDy, and with $[x_1(t)]_{**}$ the response obtained with the Extended SINDy, two RMSEs can be considered

$$RMSE_* = \sqrt{\sum_{i=1}^{i=N} \frac{\{x_1(t_i) - [x_1(t_i)]_*\}^2}{N}}$$

Eq. (21)

$$RMSE_{**} = \sqrt{\sum_{i=1}^{i=N} \frac{\{x_1(t_i) - [x_1(t_i)]_{**}\}^2}{N}}$$

Eq. (22)

2.4.1. Results of system identification of synthetic model with no noise contamination

The Extended SINDy algorithm converges to the SINDy [10] algorithm in the case of continuous motion as the stick-slip time constraints for the stops are not activated. From Table 3, it is possible to observe that the system identification is accurate with a very low value of $RMSE_{**}$. The displacement response obtained with the Extended SINDy algorithm and with SINDY are compared to the synthetic data in Fig. 2. It is possible to observe a very good agreement between the Extended SINDy and the synthetic data, while the accuracy of

SINDy is affected by the number of stops per cycle during stick-slip. It is also important to discuss the upper bound and lower bound surfaces (see Eq. (16) and Eq. (17)). From Fig. 3, it is possible to observe that they do not intersect each other at one unique point due to the errors arising from numerical differentiation of $x_1(\boldsymbol{t})$ and $x_2(\boldsymbol{t})$. The error in estimation of stiffness, viscous damping and friction force magnitude (all mass-normalized) is reported in Table 5. It is possible to observe that as the number of stops increases, the Extended SINDy display a much lower percentage relative error compared to SINDy.

Research Paper 1

Table 3 Results of system identification using synthetically generated data

Regime	Algorithm	Identified Equation	RMSE (10^{-4}m)
Continuous motion	SINDy	$\dot{x}_1 = x_2$ $\dot{x}_2 = -358.706x_1 - 0.08x_2 + 358.432u + 0.08\dot{u} - 0.085\mathrm{sgn}(x_2)$	0.014
	Extended SINDy	Converges to SINDy	-
2-stop stick-slip motion	SINDy	$\dot{x}_1 = 0.97x_2$ $\dot{x}_2 = -336.48x_1 - 0.47x_2 + 332.5u + 1.2\dot{u} - 0.015\mathrm{sgn}(x_2)$	1.06
	Extended SINDy	$\dot{x}_1 = 0.97x_2$ $\dot{x}_2 = -355.69x_1 - 0.05x_2 + 355.69u + 0.05\dot{u} - 0.08\mathrm{sgn}(x_2)$	0.01
4-stop stick-slip motion	SINDy	$\dot{x}_1 = 0.97x_2$ $\dot{x}_2 = -323.482x_1 - 0.41x_2 + 369.92u + 1.5\dot{u} - 0.025\mathrm{sgn}(x_2)$	5.4
	Extended SINDy	$\dot{x}_1 = 0.97x_2$ $\dot{x}_2 = -354.56x_1 - 0.04x_2 + 354.56u + 0.04\dot{u} - 0.083\mathrm{sgn}(x_2)$	0.05

Table 4 Values of hyperparameters used in Extended SINDy

Description of Hyperparameters	Synthetic data	Experimental data
Threshold value for STLSq	0.03	0.03
Threshold value for SR3	0.05	0.05
Cut-off velocity for mass-sticking $\left(v_{stop}\, \frac{m}{s}\right)$	10^{-7}	10^{-7}
Cut-off velocity for mass-motion $\left(v_{slip}\, \frac{m}{s}\right)$	10^{-3}	10^{-3}
Window length for smooth finite difference	35	41
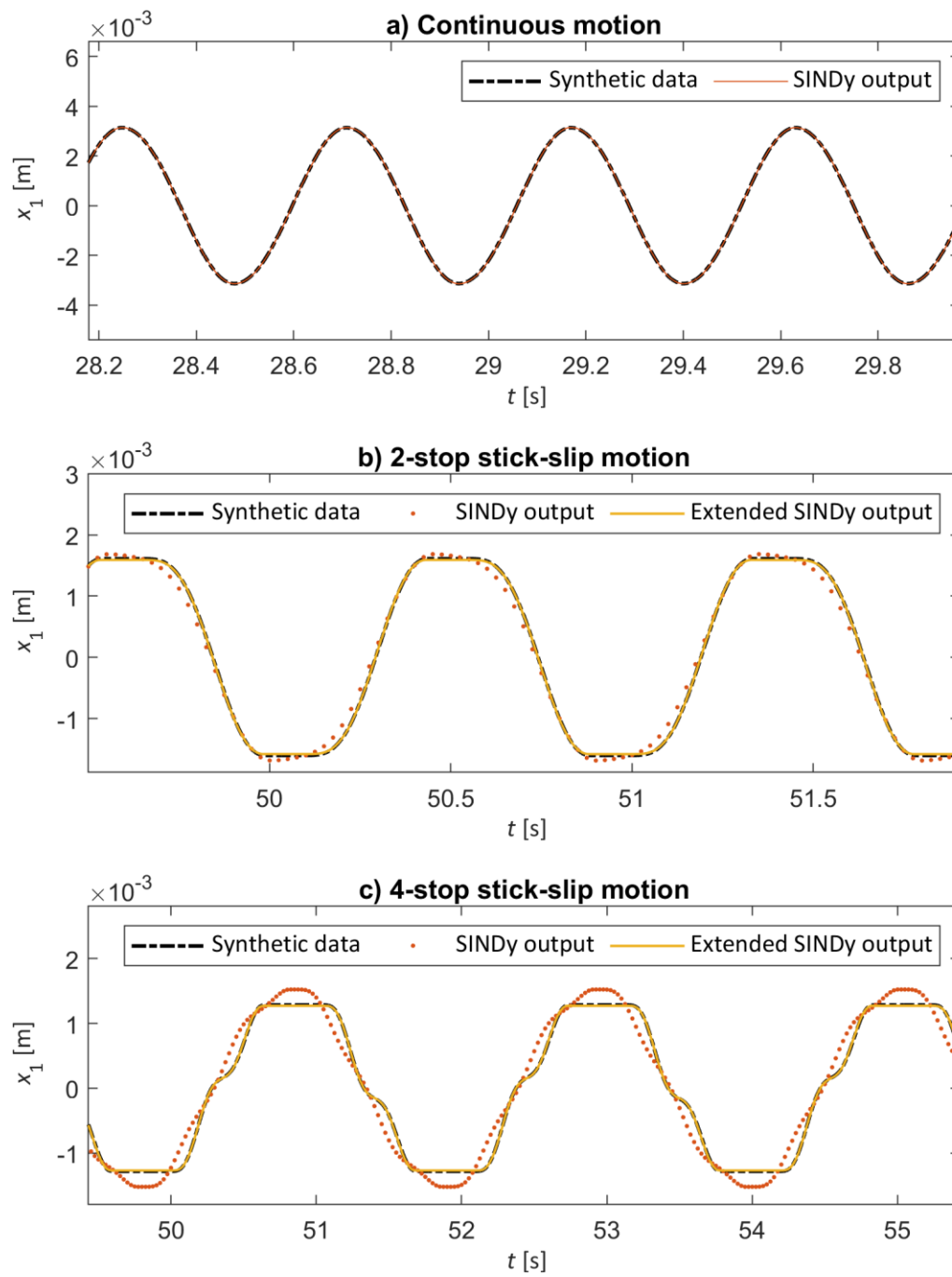
Fig. 2 Comparison between the response of the SDoF nonlinear system in the case of synthetically generated data
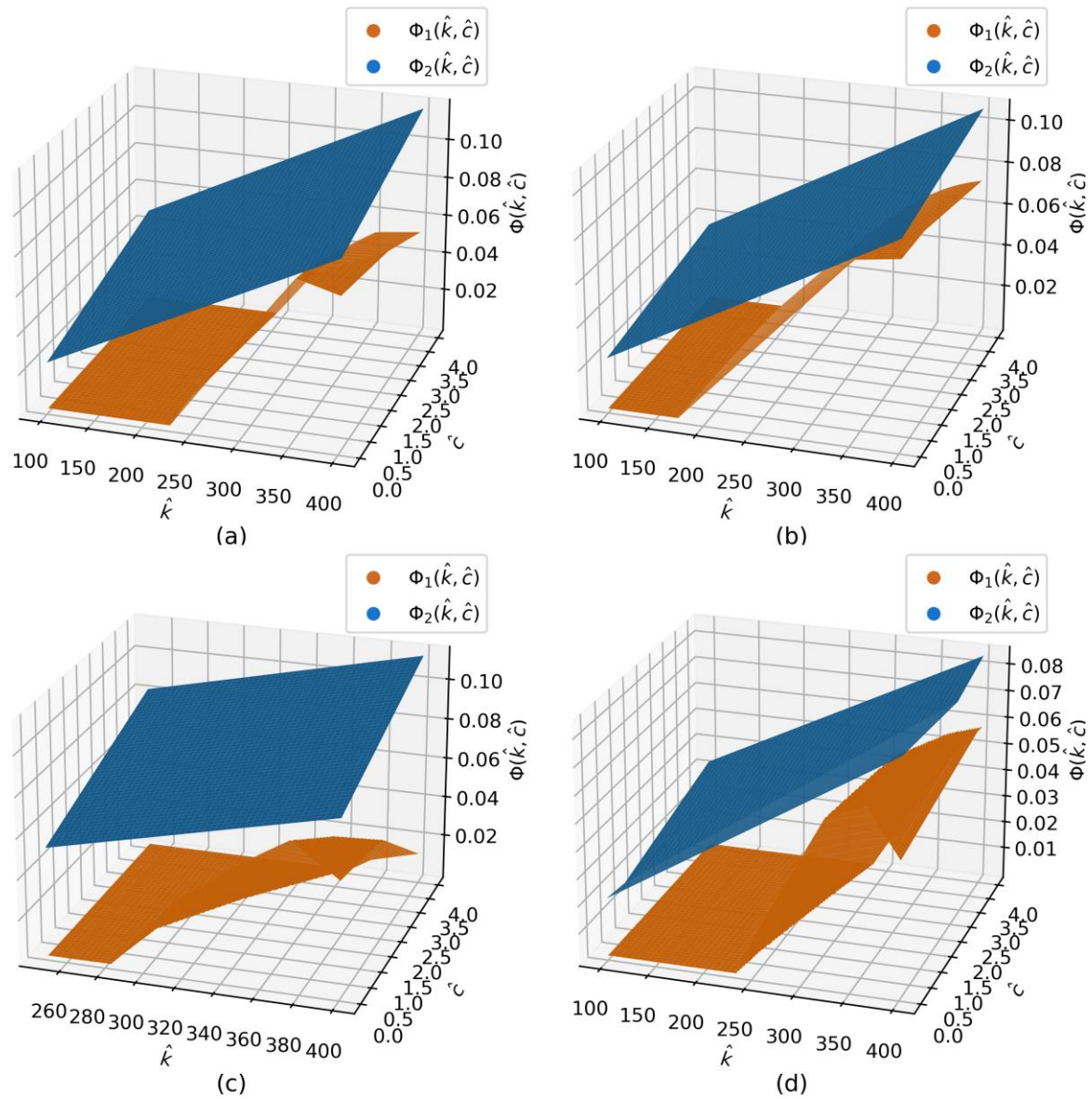
Fig. 3 Lower bound and upper bound surfaces for 2-stop stick-slip synthetic model (a) 4-stop stick-slip synthetic model (b) 2-stop stick-slip experimental model (c) 4-stop stick-slip experimental model (d)

Table 5 Relative percentage error in parameter estimation using SINDy and Extended SINDy for synthetic data

Regime	Algorithm	Relative percentage error in identification of stiffness, viscous damping, friction force magnitude (all mass-normalized) $\left(\%\frac{\Delta\hat{k}}{\hat{k}}, \%\frac{\Delta\hat{c}}{\hat{c}}, \%\frac{\Delta\hat{F}_f}{\hat{F}_f}\right)$
Continuous motion	SINDy	$0, 23.07, 0$
	Extended SINDy	Converges to SINDy
2-stop stick-slip motion	SINDy	$6.19, 623.07, 82.35$
	Extended SINDy	$0.84, 23.07, 5.88$
4-stop stick-slip motion	SINDy	$9.82, 530.7, 70.58$
	Extended SINDy	$1.15, 38.46, 2.35$

2.4.2. Effect of noise on synthetic model case study

The synthetic data is contaminated with different signal-to-noise ratio (SNR) levels to evaluate the extent of applicability of Extended SINDy algorithm. This is done by using the random.normal function from the NumPy library of Python with zero mean. The standard deviation of noise and the corresponding SNR levels are reported in Table 6. The effect of noise on dynamic system parameter estimation and RMSE is reported in Fig. 4 and Fig. 5.
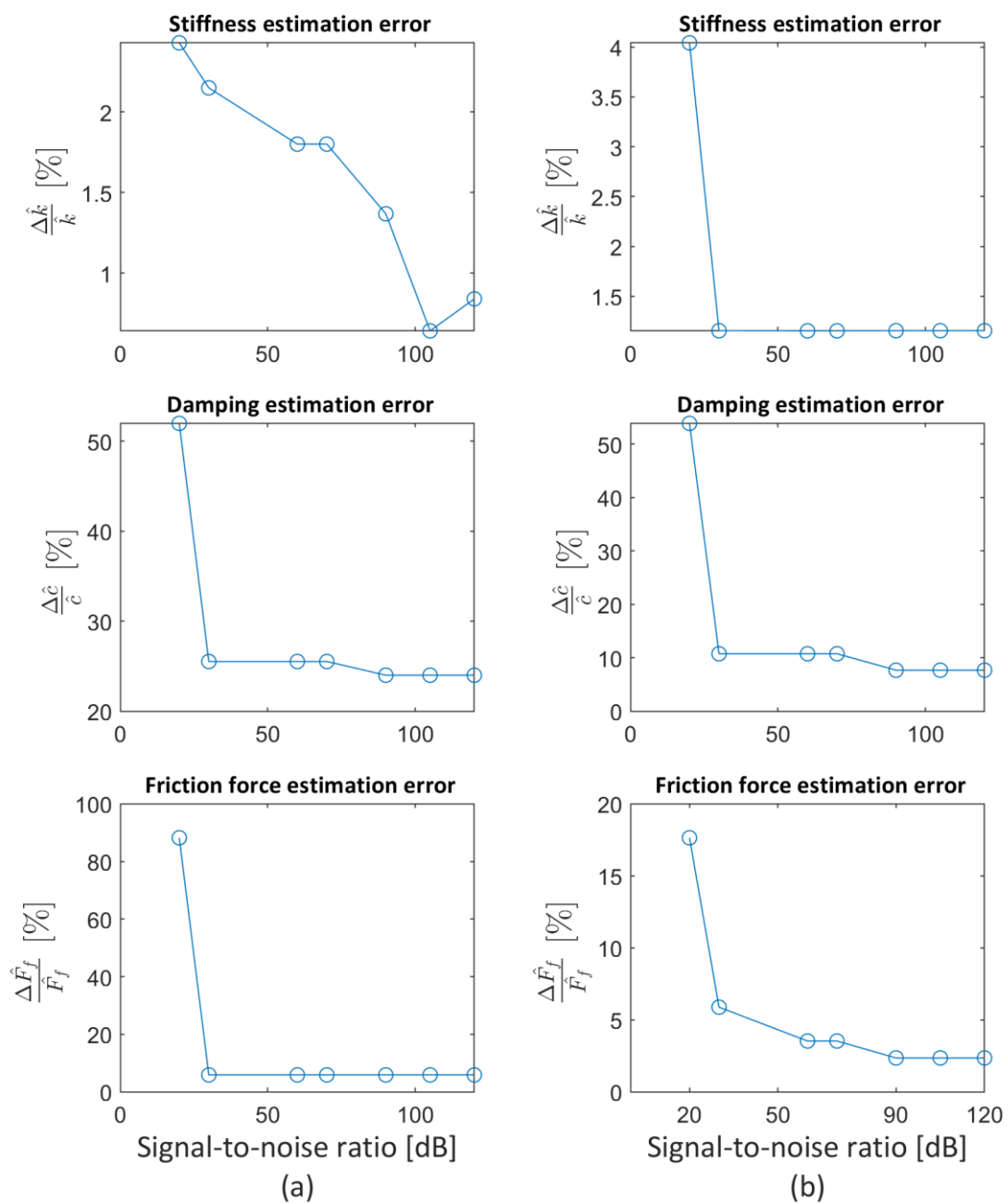
Fig. 4 Error in estimation of mass normalized stiffness, damping, and magnitude of friction force using extended SINDy for 2-stop stick-slip motion (a) and 4-stop stick-slip motion (b) in presence of different levels of noise

It is observed that below the SNR of 20 dB, the SINDy algorithm fails to identify the functional form of the EOM, therefore affecting the step 2 of the Extended SINDy. Nonetheless, it is observed that the Extended SINDy yields a lower RMSE. Above the SNR of 20 dB, the effect of noise on parameter estimation and RMSE is found within an acceptable range.

(a)   (b)
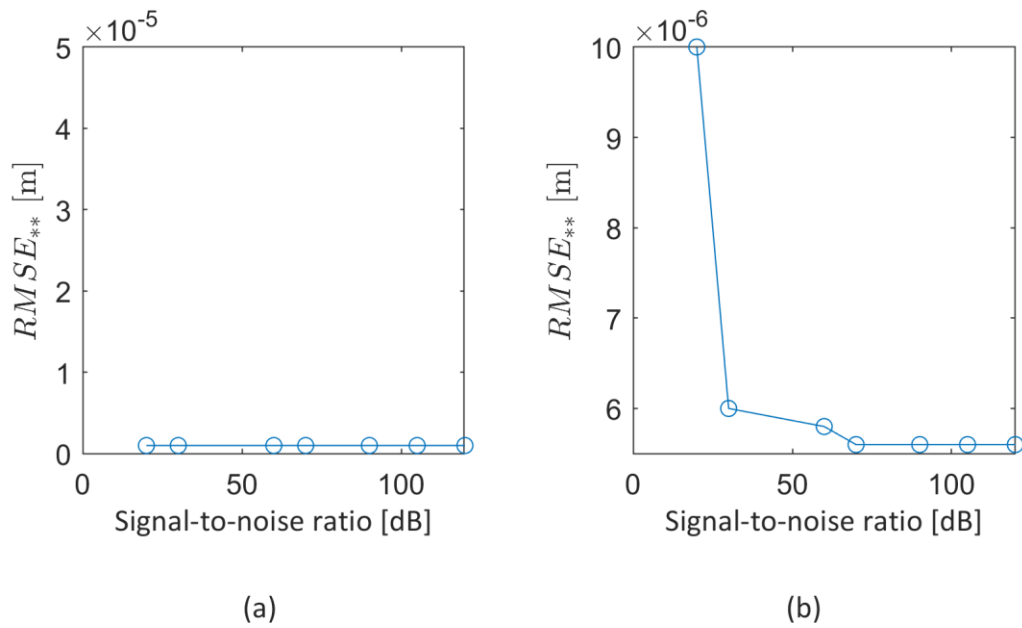
Fig. 5 Effect of noise on RMSE using Extended SINDy algorithm for 2-stop stick-slip motion (a) and 4-stop stick-slip motion (b)

Table 6 Conversion between standard deviation and signal -to-noise ratio

Standard deviation (σ) mm	Signal-to-noise ratio (dB)
1.4×10^{-2}	20
1.4×10^{-3}	30
1.4×10^{-6}	60
1.4×10^{-7}	70
1.4×10^{-9}	90
1.4×10^{-10}	105
1.4×10^{-12}	120

2.5. Experimental Model Case Study

The performance of the Extended SINDy is further evaluated by considering an experimental case study which involves a single storey frame structure with a Coulomb friction contact excited via base excitation.

2.5.1. Test rig and mechanical model

The single-storey frame is shown in Fig. 6 and it has been used in [19]. This structure consists of an Aluminium base plate connected to an electric motor via a scotch-yoke mechanism. Four thin steel bars are used to connect via bolts this base plate to a steel top plate, that represents the mass of the equivalent SDOF. The base plate is excited by using an approximately harmonic excitations generated by the electric motor. A brass disk mounted on a bar pinned to the external frame is used to produce a friction contact on the top plate. The friction force is proportional to the weight of the brass disk, and it can be adjusted by using a counterweight system. The EOM of the experimental system corresponds to Eq. (12) with parameters as specified in Table 1 – these were calculated by using free vibration tests on the experimental system with and without friction (as described in [19]). More details about the experimental system can be found in [19]. The parameter space investigated is such that the Coulomb friction model provides a good approximation of the friction force as shown in [23]. For the experimental data, the base excitation frequencies are given in Table 2 and the amplitude of base excitation is 0.0015 m.
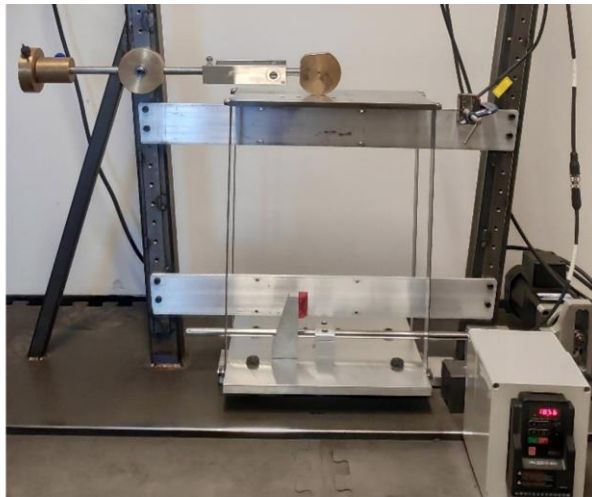
(a) Experimental setup of a SDoF with a friction contact obtained with a counter-weight system mounted on a fixed wall subject to a harmonic-based excitation
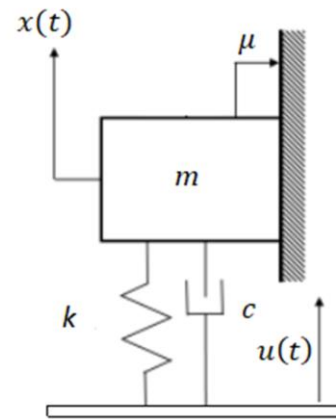
(b) Schematic representation of SDoF with friction contact

Fig. 6 SDoF dynamic system with friction as nonlinearity

2.5.2. Identification of the governing equation and results

The hyperparameters used in Extended SINDy are illustrated in Table 4. From Table 7 it can be observed that the estimated values of $\hat{k}_*, \hat{c}_*, \hat{F}_{f_*}$ obtained with the Extended SINDy provide a good approximation of terms specified in Table 1, improving the accuracy of SINDy. However, compared to the numerical simulations, these results are overall less accurate. This is because the data of $x_2(t)$, and $\dot{x}_2(t)$ are affected by the nonideal harmonic excitation, other sources of the dissipation in the experimental setup not accounted for in the mathematical model and because of additional numerical errors caused by the numerical differentiation. The difference between the results yielded by the SINDy and the Extended SINDy is not obvious in the case of 2-stop stick-slip motion reported in Fig. 7. However, a difference can be observed in terms of RMSE from Table 7. Further, from Fig. 7, it is possible to observe a notable difference between the results yielded by SINDy and Extended SINDy for 4-stop stick-slip motion. The improvement in parameter identification when using the Extended SINDy can be further observed in Table 8.

Research Paper 1

Table 7 Results of system identification using experimental data

Regime	Algorithm	Equation identified	RMSE (10^{-4}m)
Continuous motion	SINDy	$\dot{x}_1 = 0.95x_2$ $\dot{x}_2 = -397.66x_1 - 0.15x_2 + 392.56u - 0.69\dot{u}$ $- 0.031\text{sgn}(x_2)$	10.1
	Extended SINDy	Converges to SINDy	-
2-stop stick-slip motion	SINDy	$\dot{x}_1 = 0.97x_2$ $\dot{x}_2 = -362.56x_1 - 0.731x_2 + 352.1u + 1.2\dot{u}$ $- 0.015\text{sgn}(x_2)$	2.8
	Extended SINDy	$\dot{x}_1 = 0.97x_2$ $\dot{x}_2 = -365.48x_1 - 0.04x_2 + 365.48u + 0.04\dot{u}$ $- 0.08\text{sgn}(x_2)$	1.35
4-stop stick-slip motion	SINDy	$\dot{x}_1 = 0.97x_2$ $\dot{x}_2 = -371.48x_1 - 1.02x_2 + 369.7u + 1.5\dot{u}$ $- 0.002\text{sgn}(x_2)$	5.4
	Extended SINDy	$\dot{x}_1 = 0.97x_2$ $\dot{x}_2 = -364.56x_1 - 0.08x_2 + 364.56u + 0.08\dot{u}$ $- 0.065\text{sgn}(x_2)$	1.52
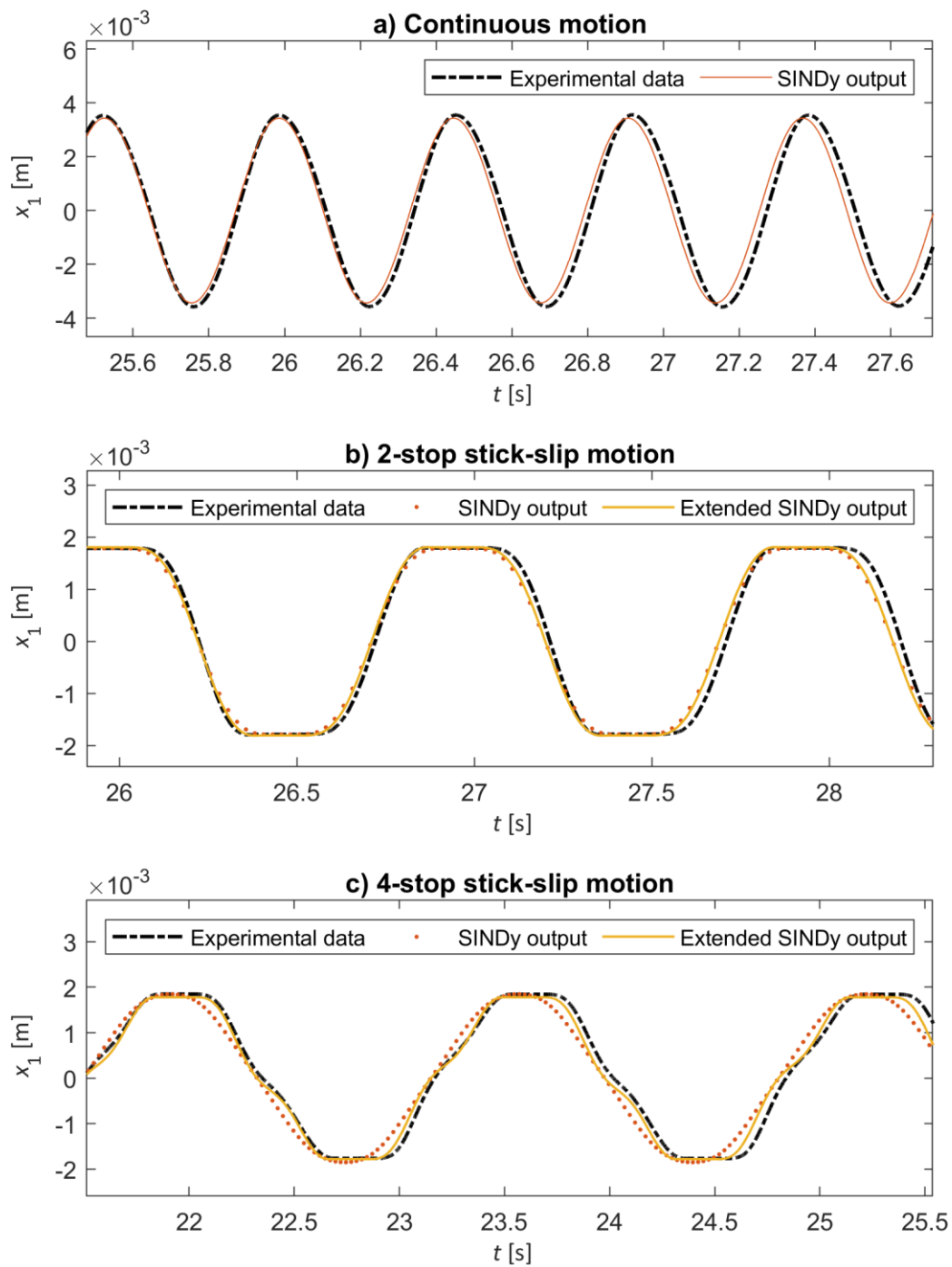
Fig. 7 Comparison between the response of the SDoF nonlinear system in the case of experimentally generated data

Research Paper 1

Table 8 Relative percentage error in parameter estimation using SINDy and Extended SINDy for experimental data

Regime	Algorithm	Relative percentage error in identification of stiffness, viscous damping, friction force magnitude (all mass-normalized) $\left(\%\frac{\Delta\hat{k}}{\hat{k}}, \%\frac{\Delta\hat{c}}{\hat{c}}, \%\frac{\Delta\widehat{F_f}}{\widehat{F_f}}\right)$
Continuous motion	SINDy	10.86, 130.76, 63.52
	Extended SINDy	Converges to SINDy
2-stop stick-slip motion	SINDy	1.074, 1024.6, 82.35
	Extended SINDy	1.88, 38.46, 5.88
4-stop stick-slip motion	SINDy	3.56, 1469.23, 97.64
	Extended SINDy	1.63, 23.07, 23.52

2.6. Conclusions

An Extended SINDy algorithm has been proposed for identifying the governing EOM of a SDoF system with friction contact subject to a harmonic excitation. It is shown that the existing SINDy approach is unable to accurately identify the epistemic uncertainty of the system parameters such as the stiffness, viscous damping, and friction force (all mass normalized) of the dynamic system. The Extended SINDy overcomes these limitations by using the SINDy algorithm on part of the data to evaluate the functional form of the governing EOM and by incorporating physics knowledge by using stick and slip temporal constraints. The last step is implemented by employing a constrained optimization strategy. The proposed Extended SINDy algorithm is applied to the data obtained from two dynamic systems, namely a synthetic SDoF oscillator with friction contact subject to a harmonic excitation and an experimental setup representing a SDoF dynamic system with steel to brass contact subject to an approximately harmonic base input. A good agreement was found between the estimated system parameters and the actual system parameters of both the above-stated systems.

The main advantage of the Extended SINDy algorithm over existing data-driven algorithms is that it can explicitly incorporate the physics constraints in the time domain. The output is in the form of an EOM and hence can be used to interpret the uncertain system parameters like stiffness, viscous damping, and nonlinear friction force, all normalized with mass. Leveraging on the SINDy algorithm, the Extended SINDy algorithm can accurately estimate the system parameters for various noise levels. It has been observed that an improved parameter estimate is obtained when using a dataset which includes the transient response (measured from zero initial conditions) and the steady state response caused by a sinusoidal load.

Although the current investigations have been limited to a non-smooth nonlinearity caused by a friction contact, the proposed approach can be generally applied to SDoF dynamic systems with discontinuous nonlinearity causing the system to show different motion behaviour which can be explicitly identified with physics constraints. Current investigations are exploring the applicability of the Extended SINDy algorithm to the

Multiple Degree of Freedom (MDoF) dynamic system with single and multiple friction contacts, and to a random external excitation.

The proposed methodology can be used in identifying the model parameters and identifying the governing EOM of a SDoF dynamic system in laboratory conditions Using the obtained EOM, a representative virtual model of the dynamic system is identified. This enables the virtual investigations of the behaviour of such system under a broad range of loading conditions that might not be possible to reproduce in laboratory conditions because of cost or time constraints. The proposed approach is a first step towards the real-time identification of nonlinearity of structural joints in operating conditions. It is worth mentioning that the implementation of more advanced numerical differentiation schemes might improve the accuracy in estimating the lower bound and upper bound surfaces. This will further improve in accurately estimating the system parameters $\hat{k}_*, \hat{c}_*, \hat{F}_{f_*}$.

Acknowledgement

Bibliography of Chapter 2

[1]   R. Bouc, "The Power Spectral Density of Response for a Strongly Non-Linear Random Oscillator", *Journal of sound and vibration,* vol. 175, pp 317-331, 1994 https://doi.org /10.1006/jsvi.1994.1331

[2]   T.K. Caughey, "Response of Van der Pol's oscillator to random excitation", *J. Appl. Mech*, vol. 26, pp. 345-348, 1960 https://doi.org/10.1115/1.4012044

[3]   T.K. Caughey, "Random Excitation of a System with Bilinear Hysteresis", *J. Appl. Mech,* vol. 27, pp. 649-652, 1960 https://doi.org/10.1115/1.3644077

[4]   T.K. Caughey, "Equivalent Linearization Techniques", *The Journal of the Acoustical Society of America,* vol. 35, pp. 1706-1711, 1963 https://doi.org/10.1121/1.1918794

[5]   C. Soize, "Stochastic Linearization Method with Random Parameters and Power Spectral Density Calculation", *Sixth International Conference on Structural Safety and Reliability*, pp. 217-22,1993

[6]   I. J. Leontaritis , and S. A. Billings, "Input-Output Parametric Models for Non-Linear Systems Part I: Deterministic Non-Linear Systems", *International journal of control*, vol. 41, pp. 329-344, 1985 https://doi.org/10.1080/0020718508961129

[7]   I. J. Leontaritis, and S. A. Billings, "*Input-output parametric models for non-linear systems part II: stochastic non-linear systems*", vol. 41, pp. 329-344, 1985 https://doi.org/10.1080/ 0020718508961130

[8]   S.A. Billings, S. Chen, and R.J. Backhouse, "The Identification of Linear and Non-Linear Models of a Turbocharged Automotive Diesel Engine", *Mechanical Systemsnd Signal Processing,* vol. 3, pp 123-142, 1989 https://doi.org/10. 1016/0888-3270(89)90012-5

[9]   G. Kerschen, K. Worden, A. F. Vakakis, and J. C. Golinval, "Past, Present and Future of Nonlinear System Identification in Structural Dynamics", *Mechanical systems and signal processing*, vol. 20, pp. 505-592, 2006 https://doi.org/10.1016/j.ymssp. 2005.04.008

[10]   S. L. Brunton, J. L Proctor, and J. N. Kutz, "Discovering Governing Equations from Data by Sparse Identification of Nonlinear Dynamical Systems", *Proceedings of the national academy of sciences,* vol. 113, pp. 3932-3937, 2016 https://doi.org/10.10

Bibliography of Chapter 2

73/pnas.151738411

[11] B. de Silva, K. Champion, M. Quade, J. Loiseau, J. N. Kutz, and S. L. Brunton, "Pysindy: A Python Package for the Sparse Identification of Nonlinear Dynamics from Data", *preprint arXiv,* 2020 https://doi.org/10.48550/arXiv.2004.08424

[12] U. Fasel, E. Kaiser, J N. Kutz, B. W. Brunton, and S. L. Brunton, "Sindy with Control: A Tutorial", *60th IEEE Conference on Decision and Control (CDC),* 2021 https://doi.org/10.1109/CDC45484.2021. 9683120

[13] M. Hoffmann, C. Frohner, and F. Noe, "Reactive SINDy: Discovering governing reactions from concentration data", *The Journal of chemical physics*, vol. 150, 2019 https://doi.org/10.1063/1.5066099

[14] S. Lakshminarayana, S. Sthapit, and C. Maple, "Application of Physics-Informed Machine Learning Techniques for Power Grid Parameter Estimation", *Sustainability*, vol. 14, 2022 https://doi.org/10.3390/su 14042051

[15] A. Sandoz, V. Ducret, G. A. Gottwald, G. Vilmart, and K. Perron, "Sindy for Delay-Differential Equations: Application to Model Bacterial Zinc Response", *Proceedings of the Royal Society*, vol. 479, 2023 https://doi.org/10.1098/rspa.2022.0556

[16] S. C. Huang, H. Chen, and M. Tien, "Predicting Nonlinear Modal Properties by Measuring Free Vibration Responses", *ASME Journal of Computational and Nonlinear Dynamics*, vol. 18, 2023 https://doi.org/10.1115/1.4056949

[17] M. Didonna, M. Stender, A. Papangelo, F. Fontanela, M. Ciavarella, and N. Hoffmann, "Reconstruction of Governing Equations from Vibration Measurements for Geometrically Nonlinear Systems", *Lubricants,* vol. 8, 2019 https://doi.org/10.3390/lubricants7 080064

[18] R. C. Hilborn, "*Chaos and Nonlinear Dynamics: An Introduction for Scientists and Engineers*", Oxford University Press, 2000 https://doi.org/10.1063/1.4823351

[19] L. Marino, and A. Cicirello, "Experimental Investigation of a Single-Degree-of-Freedom System with Coulomb Friction", *Nonlinear Dynamics*, vol. 99, pp. 1781-1799, 2020 https://doi.org/10.1007/s11071-019-05443-2

[20] MATLAB, version 9.9.0.1857802 (R2020b). The Mathworks Inc (2020)

[21] L. Marino, Alice Cicirello, and David A. Hills. "Displacement transmisibiltiy of a Coulomb friction oscillator subject to joined base-wall motion." *Nonlinear Dynamics*

Bibliography of Chapter 2

98, no. 4 (2019): 2595-612. https://doi.org/10.1007/s11071-019-04983-x

[22]   P. Zheng, T. Askham, S. L. Brunton, J. N. Kutz, and A. Y. Aravkin, "A Unified Framework for Sparse Relaxed Regularized Regression: Sr3", *IEEE Access* 7, *pp. 1404-1423, 2018* https://doi.org/10.1109/ACCESS.2018.2886528

[23]   A. Cabboi, L. Marino, A. Cicirello, "A Comparative Study between Amontons– Coulomb and Dieterich–Ruina Friction Laws for the Cyclic Response of a Single Degree of Freedom System", *European Journal of Mechanics -A/Solids,* vol. 96, 2022 https://doi.org/10.1016/j. euromechsol.2022.104737

List Of Figures In Chapter 3

List Of Tables In Chapter 3

3. Research Paper 2

Governing equations identification for moment-rotation relationship of pinned column base-plate connections using the Dahl model with varying parameter

Saurabh Mahajan[1], Florentia Kavoura[1]

[1] Faculty of Civil Engineering and Geosciences

Delft University of Technology,

Delft, 2628 CN, South Holland, The Netherlands.

Abstract

The pinned column base-plate connections experience hysteresis when loaded in the elastic region. This study proposes an approach to represent the hysteretic moment-rotation relationship in the time domain. Precisely, an unsymmetric hysteresis is investigated both numerically and experimentally. The methodology consists of (i) collecting and segregating the moment-rotation data into different branches of hysteresis (ii) schematic representation of experimental setup (iii) using the Dahl model with different slope parameter for each branch of hysteresis and estimating the parameter using Bayesian Optimization. It is shown that the Dahl model with different slope parameter for each branch of hysteresis yields moment-rotation diagram with good accuracy when compared with the numerical and experimental moment-rotation data.

Keywords: Pinned column base-plate connection, Unsymmetric hysteresis, Dahl model, Bayesian Optimization

3.1. Introduction

Buildings are subject to dynamic loading due to earthquakes and wind. The response of the structure subject to dynamic load depends on its lateral and rotational stiffness. Dynamic loads affect high-rise as well as low-rise buildings. Many times, low-rise structures (e.g. warehouses, retail stores, libraries) are built considering their cost-effectiveness. Hence, an understanding of the strength design of low-rise structures is important. The strength design and serviceability of the building structure are influenced by the moment capacity

and the rotational stiffness of the column-to-foundation connections. In the case of low-rise buildings, the column-to-foundation connection is pinned. Hence, while performing design calculations, the rotational stiffness of the connection is considered zero.

However, due to the large size of the pinned connection, it may provide a non-trivial rotational stiffness [1-4]. This non-trivial rotational stiffness will increase the design strength of the connection as well as the structure. Hence, to design the structure with good accuracy, it is important to study the moment-rotation behaviour of the pinned column-to-foundation connections. The existing models for representing the moment-rotation curves can be broadly divided into (i) Models depending on parameters with clear physical meaning (e.g. stiffness, resistance) and a shape factor [5]. The well-known examples of these models are the linear model [6], the bilinear model [7-9], and the nonlinear model [10]. (ii) Models relying on formulation based on curve fitting by regression analysis [5].

Although the above-mentioned models give a good approximation of moment-rotation curves, they are time-invariant. The rotational stiffness varies in time when the connection is subject to external dynamic loading. This is observed when the pinned column-to-foundation connection is loaded in an elastic or inelastic region [11]. Further, the loss of energy (hysteresis) is observed when the connection is subject to an external loading in an elastic or inelastic region. An elastic and inelastic region is when the stresses in the material of the connection are below and above the yield point respectively. The possible reason for the loss of energy in an elastic region is due to the heat generated due to loading and unloading [12]. Furthermore, due to the different maximum positive and negative values of the hysteretic moment, the observed moment-rotation hysteresis diagram is unsymmetric. Hence, to accurately represent the unsymmetric moment-rotation relationship in the time domain, it is necessary to have a time-dependent functional form of the moment-rotation curve.

In this study, the governing equation is proposed for representing the unsymmetric moment-rotation relationship in the time domain. This is done by segregating the moment-rotation hysteretic data into positive increasing, positive decreasing, negative increasing, and negative decreasing branches. The positive increasing branch indicates the moment is positive and the magnitude of rotation is increasing, positive decreasing branch denotes a positive moment and decreasing magnitude of rotation. Similarly, the negative increasing

branch represents that the moment is negative and the magnitude of rotation is increasing, the negative decreasing branch denotes negative moment and decreasing magnitude of rotation. As the experimental data has an issue of low sampling frequency, a synthetic moment-rotation hysteresis data is generated using the Bouc-Wen model of hysteresis [13], [14]. Further, the experimental setup of pinned column base-plate connection is represented as an equivalent rotational Single Degree of Freedom (SDoF) with restoring hysteretic moment. Furthermore, the Dahl model [15] with different slope parameter for each branch of hysteresis is considered. The next step consists of using the considered Dahl model to validate the restoring hysteretic moment-rotation diagram generated by the Bouc-Wen model of hysteresis. The slope parameter for the different branches of the Dahl model is estimated using Bayesian Optimization [16]. The Dahl model with different slope parameter for each branch is later used to identify the governing equation for the experimental data of three different pinned column base-plate connections.

3.2. Experimental Setup and Data Segregation

3.2.1. Experimental setup

As shown in   Fig. 1 the experimental setup consists of a pinned column base-plate connection resting on the concrete foundation and it has been used in [11]. The base-plate and the concrete foundation are connected via anchor rods.
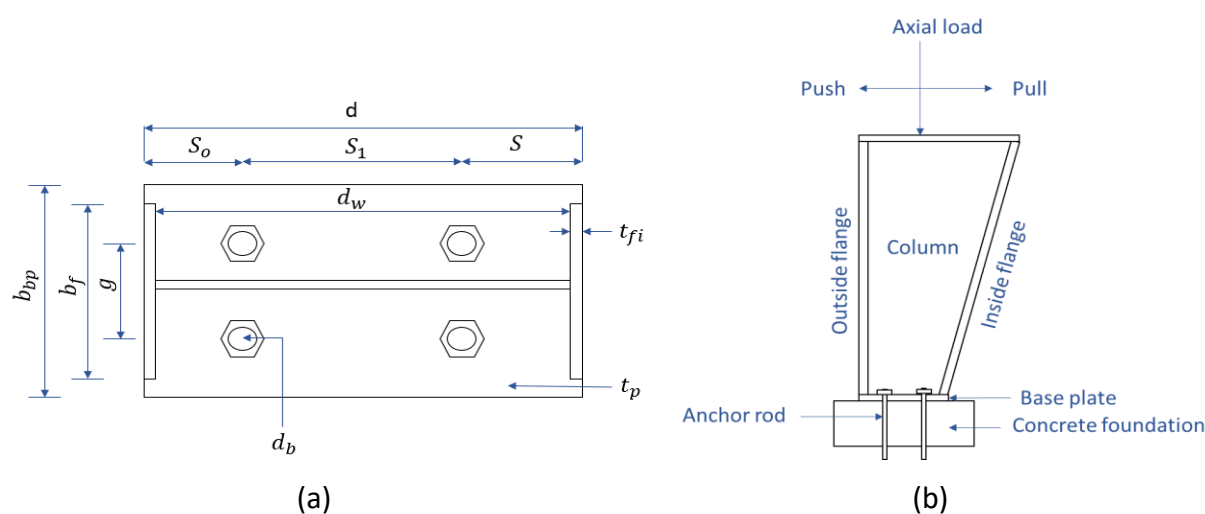
Fig. 1 Top view (a) and Front view (b) of Pinned column base-plate connection

Research Paper 2

The connection is loaded by applying the cyclic displacements at the top of the column as shown in Fig. 1. Additionally, an axial load of 222 KN was applied at the top of the column to take second-order moments into consideration. Further, the resisting moment is defined as the sum of the first-order and second-order moments. The resulting rotation at the bottom of the connection is recorded using the potentiometers. Three different specimens (S01, S03, and S07 of [11]) were considered for finding the governing equation for representing the unsymmetric moment-rotation relationship in the time domain.

(a)

(b)
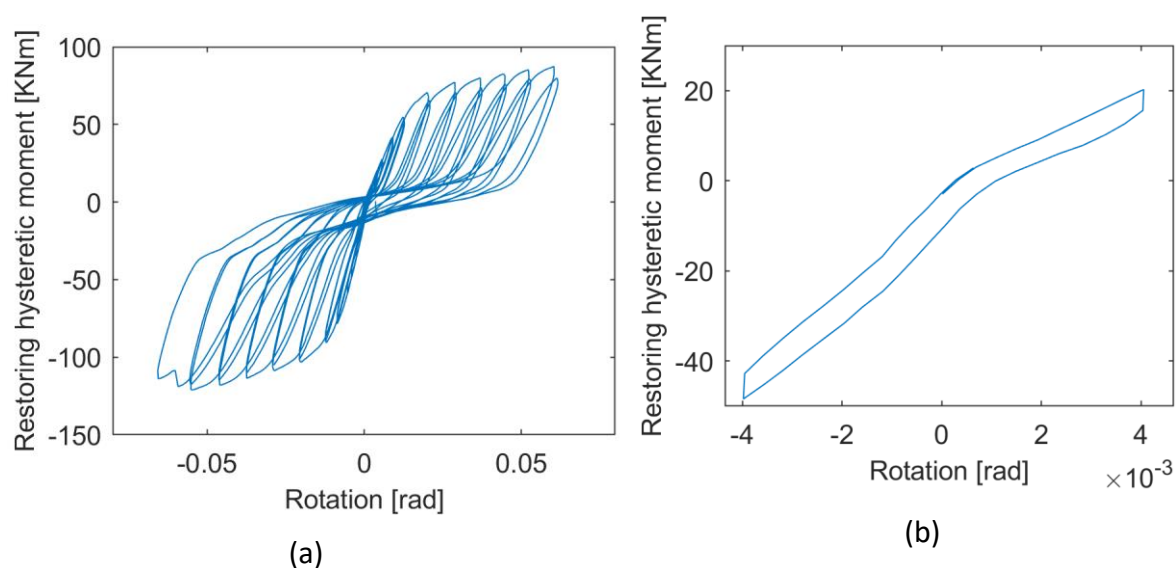
Fig. 2 Restoring hysteretic moment-rotation diagram of S03 in an elastic and inelastic region (a) and elastic region (b)

The hysteretic restoring moment-rotation diagram for S03 is reported in Fig. 2 (a). Further, as the study is in the primary stage, the hysteresis loop in the elastic region is considered for estimating the governing equation.

Table 1 Details of experimental base-plate connection

Spec-imen	d_w	b_f	t_{fo}	t_{f1}	b_{bp}	d	t_w	t_p	d_b	g	S_0	S_1	S
S01	304.8	203.2	6.4	9.5	203.2	320.7	4.7	15.9	19.1	101.6	76.2	101.6	15.8
S03	304.8	203.2	6.4	9.5	203.2	320.7	4.7	25.4	19.1	101.6	101.6	101.6	117.5
S07	558.8	355.6	12.7	15.9	355.6	587.4	6.4	15.9	31.8	127	101.6	127	231.8

The hysteresis loop in the elastic region is shown in Fig. 2 (b). The geometrical description of these connections is stated in Table 1. More details about the experimental specimen, instrumentation, and material properties can be found in [11]. The next step involves segregating the moment-rotation dataset into positive increasing, positive decreasing, negative increasing, and negative decreasing branches.

3.2.2. Data segregation

Let $m(t)$ and $\theta(t)$ denote the restoring hysteretic moment and angular displacement, respectively, of the pinned column base-plate connection. The time vector is represented as

$$\boldsymbol{t} = [t_1 \ t_2 \dots t_{nd}], t_1 = 0 \ \& \ t_{nd} = T \qquad \text{Eq. (1)}$$

Where, T is the time period of one cycle of angular displacement. The moment-rotation data of the experimental setup is segregated by applying conditions based on moment and rotation as

$$\begin{cases} m(\boldsymbol{t}) > 0 \ and \ \theta(t_i) < \theta(t_{i+1}) \rightarrow t \epsilon t_{PI} \rightarrow \boldsymbol{m_{PI}} = m(\boldsymbol{t_{PI}}), \boldsymbol{\theta_{PI}} = \theta(\boldsymbol{t_{PI}}) \qquad \text{Eq. (2)} \\ \boldsymbol{t_{PI}} = [t_1 \ t_2 \dots t_{pi}] \end{cases}$$

$$\begin{cases} m(\boldsymbol{t}) > 0 \ and \ \theta(t_i) > \theta(t_{i+1}) \rightarrow t \epsilon t_{PD} \rightarrow \boldsymbol{m_{PD}} = m(\boldsymbol{t_{PD}}), \boldsymbol{\theta_{PD}} = \theta(\boldsymbol{t_{PD}}) \qquad \text{Eq. (3)} \\ \boldsymbol{t_{PD}} = [t_{pi+1} \ t_{pi+2} \dots t_{pd}] \end{cases}$$

$$\begin{cases} m(\boldsymbol{t}) < 0 \ and \ \theta(t_i) > \theta(t_{i+1}) \rightarrow t \epsilon t_{NI} \rightarrow \boldsymbol{m_{NI}} = m(\boldsymbol{t_{NI}}), \boldsymbol{\theta_{NI}} = \theta(\boldsymbol{t_{NI}}) \qquad \text{Eq. (4)} \\ \boldsymbol{t_{NI}} = [t_{pd+1} \ t_{pi+2} \dots t_{ni}] \end{cases}$$

$$\begin{cases} m(\boldsymbol{t}) < 0 \ and \ \theta(t_i) < \theta(t_{i+1}) \rightarrow t \epsilon t_{ND} \rightarrow \boldsymbol{m_{ND}} = m(\boldsymbol{t_{ND}}), \boldsymbol{\theta_{ND}} = \theta(\boldsymbol{t_{ND}}) \qquad \text{Eq. (5)} \\ \boldsymbol{t_{ND}} = [t_{ni+1} \ t_{pi+2} \dots t_{nd}] \end{cases}$$

Where, $\boldsymbol{t_{PI}}, \boldsymbol{t_{PD}}, \boldsymbol{t_{NI}},$ and $\boldsymbol{t_{ND}}$ represent time corresponding to positive increasing, positive decreasing, negative increasing, and negative decreasing branches respectively.

The hysteresis observed in the moment-rotation data of the experimental setup has an unsymmetric shape (see Fig. 2 (b)). Further, due to the large sampling time (1 second), while collecting the experimental moment-rotation data, a few data points are missing. This can be seen in the region where the positive increasing branch of hysteresis connects the positive decreasing branch, and the negative increasing branch connects the negative decreasing branch. Hence, it is important to consider an existing hysteresis model to generate an unsymmetric moment-rotation diagram without the error of time sampling.

Additionally, the moment-rotation diagram generated by the considered hysteresis model is validated using the Dahl model [15] with different slope parameter for each branch of hysteresis. To estimate the governing equation for pinned column base-plate connection, the next step involves a schematic representation of the experimental setup.

3.3. Schematic Representation and Generating Synthetic Data Using The Bouc-Wen Model

3.3.1. Schematic representation of the experimental setup

As the column base-plate connection is pinned, it has a rotational degree of freedom. As the dynamic displacements and axial load are applied at the top of the column, the external moments experienced by the connection are difficult to estimate due to their complex geometry. Further, the restoring moment of pinned column base-plate connection is hysteretic (see Fig. 2 (b). Considering all the above-mentioned characteristics, the pinned column base-plate connection is represented as a rotational SDoF dynamic system with restoring hysteretic moment. The schematic representation of the pinned column base-plate connection is shown in Fig. 3.
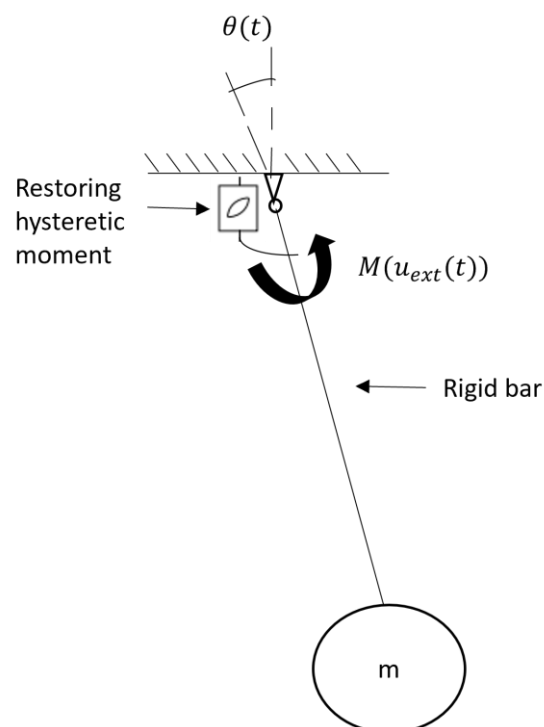
Fig. 3 Schematic representation of pinned column base-plate connection

The Equation Of Motion (EOM) of a dynamic system shown in Fig. 3 is

$$I\ddot{\theta}(t) + m_h(\theta, t) = M(u_{ext}(t)) \qquad \text{Eq. (6)}$$

Where, $\theta(t)$ is the angular displacement of the of the rotational SDoF dynamic system as well as the experimental pinned column base-plate connection. The restoring hysteretic moment in the experimental setup is represented as $m_h(\theta, t)$ in the rotational SDoF dynamic system. The external moment experienced by the pinned column base-plate connection is denoted as $M(u_{ext}(t))$. Further, I and $\ddot{\theta}(t)$ represent polar moment of inertia associated with the mass m and angular acceleration respectively. Further, as stated in 3.2.2, the Bouc-Wen model of hysteresis is considered for generating the synthetic moment-rotation data.

3.3.2. Bouc-Wen hysteresis model

For generating an unsymmetric moment-rotation diagram, the most commonly used Bouc-Wen model of hysteresis [13], [14] is used. This model is selected because it can yield an unsymmetric hysteretic moment-rotation diagram. The procedure for the same is stated in the following text.

Consider a rotational SDoF dynamic system with restoring hysteretic moment as shown in Fig. 3. The EOM of the same is given by

$$I\ddot{\theta}(t) + m_h\big(\theta(t), \dot{\theta}(t), z(t)\big) = M(u_{ext}(t)) \qquad \text{Eq. (7)}$$

Let $m_h\big(\theta(t), \dot{\theta}(t), z(t)\big)$ be the restoring hysteretic moment defined by the Bouc-Wen model of hysteresis. Further, $z(t)$ is an internal variable representing material properties. The other parameters have the same meaning as stated in Eq. (6). The hysteretic moment using the Bouc-Wen model and the internal variable representing material properties are given by [17]

$$m_h[\theta(t), \dot{\theta}(t), z(t)] = \alpha k_o \theta(t) + (1 - \alpha) k_o z(t) \qquad \text{Eq. (8)}$$

$$\begin{cases} \dfrac{dz(t)}{dt} = \dot{\theta}(t)\{B - |z(t)|^n \psi[\theta(t), \dot{\theta}(t), z(t)]\} \\ \qquad B = B_1 \; \forall \; z(t) \geq 0 \\ \qquad B = B_2 \; \forall \; z(t) < 0 \end{cases} \qquad \text{Eq. (9)}$$

Where k_o and α denote the initial stiffness of the material and post to preyield stiffness ratio respectively. B and n are the parameters that control the scale and sharpness of the

hysteresis loops. The two different values of B are adopted to create an unsymmetric hysteretic moment-rotation diagram. The ψ function of the Bouc-Wen model is represented as [17]

$$\psi[\theta(t), \dot{\theta}(t), z(t)] = \gamma + \beta \mathrm{sgn}(\dot{\theta}(t)z(t)) \qquad \text{Eq. (10)}$$

Where γ and β are the parameters controlling the shape of hysteresis loops. sgn(.) denotes the signum function. Further, Eq. (9) is integrated in MATLAB using the *ode45* function [18] and $m_h[\theta(t), \dot{\theta}(t), z(t)]$ is calculated using Eq. (8) and Eq. (11).

$$\theta(t) = A\sin(\omega t) \qquad \text{Eq. (11)}$$

The values of all the parameters of the Bouc-Wen model are calibrated and further stated in Table 2.

Table 2 Parameters of the Bouc-Wen model

Parameter	Value
A	0.0044
ω	0.216
k_o	5000
α	0.85
B_1	1
B_2	1.5
n	0.41
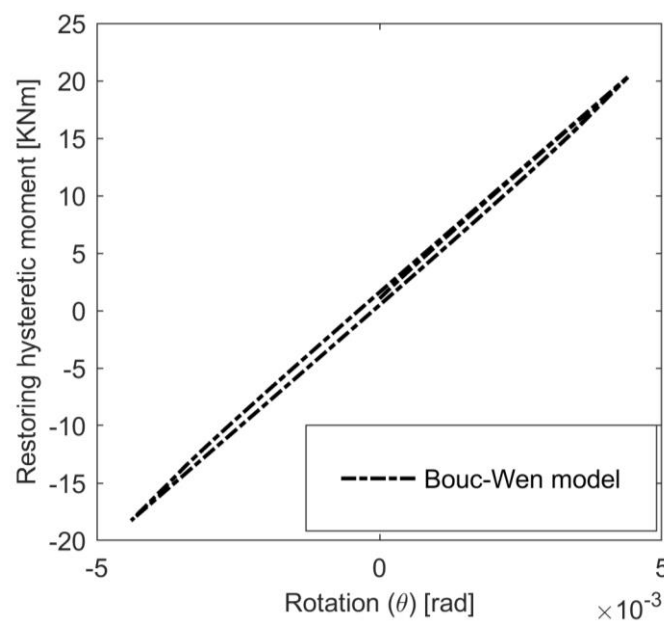
Fig. 4 Restoring hysteretic moment-rotation diagram of the Bouc-Wen model

The moment-rotation diagram using the Bouc-Wen model is shown in Fig. 4. The hysteretic moment-rotation diagram is unsymmetric as the maximum positive and maximum negative moments are different.

The Dahl model [15] with different slope parameter for each branch of hysteresis is employed for estimating an unsymmetric hysteretic moment-rotation diagram generated using the Bouc-Wen model. In particular, the Dahl model is used because it is the simplest rate-and-state model. Further, the Dahl model has the least number of parameters and hence the slope of the Dahl model can be controlled by varying the parameter associated with the slope.

3.4. Parameter Estimation Of The Dahl Model Using Bayesian Optimization

The Dahl friction model was formulated by Dahl [15] for studying the effects of nonlinear friction in ball bearings [19] under the action of an external load. The ball bearing will initially provide an elastic resistance and return to its initial position after the load is removed; however, if the load exceeds its elastic resistance, the entire ball bearing will move. The Dahl friction resistance (F) in the ball bearings is represented as [19].

$$\frac{dF}{dx} = \sigma \left| 1 - \frac{F}{F_c} \mathrm{sgn}(\dot{x}(t)) \right|^{i} \mathrm{sgn}\left(1 - \frac{F}{F_c} \mathrm{sgn}(\dot{x}(t)) \right) \qquad \text{Eq. (12)}$$

Where σ denotes the slope of force to displacement curve. F_c represents sliding Coulomb friction force. Further, i, x and $\dot{x}(t)$ denote the shape factor, displacement, and velocity, respectively, of a ball bearing. Additionally, the influence of i on the hysteresis curve is shown in Fig. 5. The Dahl model can be expressed in terms of the time derivatives as [19]

$$\frac{dF}{dt} = \frac{dF}{dx} \cdot \frac{dx}{dt} = \sigma \dot{x}(t) \left| 1 - \frac{F}{F_c} \mathrm{sgn}(\dot{x}(t)) \right|^{i} \mathrm{sgn}\left(1 - \frac{F}{F_c} \mathrm{sgn}(\dot{x}(t)) \right) \qquad \text{Eq. (13)}$$
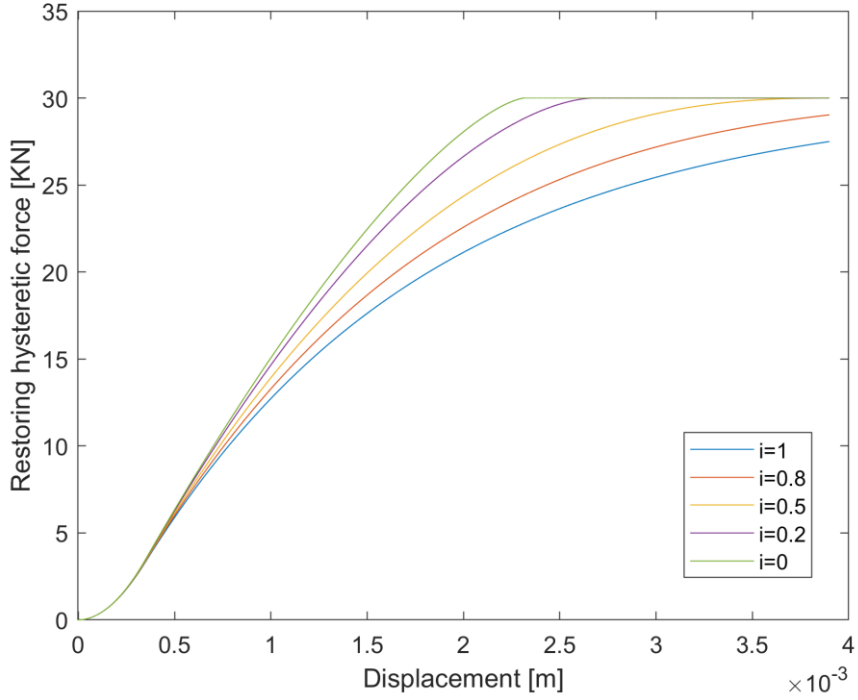
Fig. 5 Effect of i on the Dahl model

3.4.1. Dahl model for investigating hysteresis

The Dahl model is used for studying the hysteresis in materials subject to cyclic loading [20]. Due to cyclic loading, the shear stress (τ) and strain (γ) generated in the material are shown in the form of the Dahl model as [20]

$$\frac{d\tau}{d\gamma} = \frac{\sigma_\tau}{\tau_c}\left(\tau_c - \tau\,\mathrm{sgn}\,(\dot{\gamma})\right)^i \qquad \text{Eq. (14)}$$

$$\frac{d\tau}{dt} = \frac{\sigma}{\tau_c}\dot{\gamma}\left(\tau_c - \tau\,\mathrm{sgn}\,(\dot{\gamma})\right)^i \qquad \text{Eq. (15)}$$

Where σ_τ represents the slope of the stress-strain curve, τ_c is the yield limit of the material and i denotes the shape of the hysteresis loop. Therefore, in this study, the Dahl model with different slope parameter (κ) for each branch of hysteresis is used to represent the restoring hysteretic moment in the rotational SDoF dynamic system (see Fig. 3). The EOM of rotational SDoF with restoring hysteretic moment is

$$I\ddot{\theta}(t) + m_d(\theta, \boldsymbol{t}, \kappa) = M(u_{ext}(\boldsymbol{t})) \qquad \text{Eq. (16)}$$

$$\begin{cases} \dfrac{dm_d(\theta, t, \kappa)}{dt} = \kappa\dot{\theta}(t)\left(1 - \dfrac{m_d(t)}{M_c}\,\text{sgn}\left(\dot{\theta}(t)\right)\right)^i \text{sgn}\left(1 - \dfrac{m_d(t)}{M_c}\,\text{sgn}\left(\dot{\theta}(t)\right)\right) \\ \qquad\qquad \kappa = \hat{\kappa}^* \,\forall\, t = t_{PI} \\ \qquad\qquad \kappa = \hat{\kappa}^{**} \,\forall\, t = t_{PD} \\ \qquad\qquad \kappa = \hat{\kappa}^{***} \,\forall\, t = t_{NI} \\ \qquad\qquad \kappa = \hat{\kappa}^{****} \,\forall\, t = t_{ND} \end{cases} \qquad \text{Eq. (17)}$$

Where $m_d(\theta, t, \kappa)$ is the restoring hysteretic moment using the Dahl model. κ denotes the slope of the hysteretic moment rotation diagram. From the available data of moment-rotation, M_c represents the magnitude of a maximum value of moment. The other parameters have the same meaning as stated in Eq. (2)-Eq. (6). The Dahl moment $[m_d(\theta, t, \kappa)]$ is estimated by integrating Eq. (17) in MATLAB using *ode45* function [18]. Let $\hat{\kappa}^*, \hat{\kappa}^{**}, \hat{\kappa}^{***}$, and $\hat{\kappa}^{****}$ be the optimum values of the slope parameters $\kappa^*, \kappa^{**}, \kappa^{***}$, and κ^{****}. The optimum values are estimated using Bayesian Optimization [21]. Further, the variables can be represented as follows:

$$\begin{cases} \kappa^* = [\kappa_1^* \ \kappa_2^* \ \dots \ \kappa_n^*] \\ \kappa^{**} = [\kappa_1^{**} \ \kappa_2^{**} \ \dots \ \kappa_n^{**}] \\ \kappa^{***} = [\kappa_1^{***} \ \kappa_2^{***} \ \dots \ \kappa_n^{***}] \\ \kappa^{****} = [\kappa_1^{****} \ \kappa_2^{****} \ \dots \ \kappa_n^{****}] \end{cases} \qquad \text{Eq. (18)}$$

Let $M(t)$ be the available data of restoring hysteretic moment. The selection of the optimum value of the slope parameter will result in a minimum error between the moment generated using the Dahl model [15] and the available data of restoring hysteretic moment. Hence the objective function $(w(\kappa_j^*))$ is defined as the root mean square error between the available data of restoring hysteretic moment $(M(t))$ and the restoring Dahl moment $(m_d(\theta, t, \kappa))$. The objective function for estimating the parameter of a different branch of hysteresis are stated in Table 3.

Further, $M(t)$ is replaced by $m_h[\theta(t), \dot{\theta}(t), z(t)]$ for comparing the Dahl model [15] hysteresis with the Bouc-Wen model [13], [14] hysteresis. Additionally, the order (i) chosen for comparison with the Bouc-Wen model is 0.15. For comparison of the hysteretic moment-rotation data generated using the Dahl model with experimental moment-rotation data, $M(t)$ is replaced by $m(t)$ and the order (i) is 1. It is worth mentioning that the procedure followed for data segregation in the case of the Bouc-Wen model is the same as stated in section 3.2.2.

Research Paper 2

Table 3 Objective function for estimating the optimum slope parameters

Objective function

$$\begin{cases} w\left(\kappa_j^*\right) = \sqrt{\dfrac{\sum_{i=1}^{i=pi}\left[M(t_i) - m_d\left(\theta, t_i, k_j^*\right)\right]^2}{pi}} \\ \quad w(\boldsymbol{\kappa}^*) = [w(\kappa_1^*), w(\kappa_2^*), \dots, w(\kappa_n^*)] \\ \qquad (\hat{\kappa}^*) = \underset{\boldsymbol{\kappa}^*}{argmin}[w(\boldsymbol{\kappa}^*)] \end{cases}$$

$$\begin{cases} w\left(\kappa_j^{**}\right) = \sqrt{\dfrac{\sum_{i=1}^{i=pd}\left[M(t_i) - m_d\left(\theta, t_i, k_j^{**}\right)\right]^2}{pd}} \\ \quad w(\boldsymbol{\kappa}^{**}) = [w(\kappa_1^{**}), w(\kappa_2^{**}), \dots, w(\kappa_n^{**})] \\ \qquad (\hat{\kappa}^{**}) = \underset{\boldsymbol{\kappa}^{**}}{argmin}[w(\boldsymbol{\kappa}^{**})] \end{cases}$$

$$\begin{cases} w\left(\kappa_j^{***}\right) = \sqrt{\dfrac{\sum_{i=1}^{i=ni}\left[M(t_i) - m_d\left(\theta, t_i, k_j^{***}\right)\right]^2}{ni}} \\ \quad w(\boldsymbol{\kappa}^{***}) = [w(\kappa_1^{***}), w(\kappa_2^{***}), \dots, w(\kappa_n^{***})] \\ \qquad (\hat{\kappa}^{***}) = \underset{\boldsymbol{\kappa}^{***}}{argmin}[w(\boldsymbol{\kappa}^{***})] \end{cases}$$

$$\begin{cases} w\left(\kappa_j^{****}\right) = \sqrt{\dfrac{\sum_{i=1}^{i=nd}\left[M(t_i) - m_d\left(\theta, t_i, k_j^{****}\right)\right]^2}{nd}} \\ \quad w(\boldsymbol{\kappa}^{****}) = [w(\kappa_1^{****}), w(\kappa_2^{****}), \dots, w(\kappa_n^{****})] \\ \qquad (\hat{\kappa}^{****}) = \underset{\boldsymbol{\kappa}^{****}}{argmin}[w(\boldsymbol{\kappa}^{****})] \end{cases}$$

The procedure for estimating the optimum value of $\boldsymbol{\kappa}^*$ is illustrated in the following text. The same procedure is adopted for estimating the optimum value of $\boldsymbol{\kappa}^{**}$, $\boldsymbol{\kappa}^{***}$, and $\boldsymbol{\kappa}^{****}$. It is worth mentioning that first $\hat{\kappa}^*$ is estimated and later $\hat{\kappa}^{**}$, $\hat{\kappa}^{***}$, and $\hat{\kappa}^{****}$ are estimated one at a time using the objective functions mentioned in Table 3. The objective functions represent the root mean square error over different time intervals. The value of objective function $w(\boldsymbol{\kappa}^*)$ is assumed to be a Gaussian random variable for each value of $\boldsymbol{\kappa}^*$. Hence the objective function can be modeled as a Gaussian process [21]. Further, the objective function is divided into two parts (i) $\boldsymbol{w_o}$:points where the value of $\boldsymbol{w}$ is known (noise-free observations) and (ii) $\boldsymbol{w_*}$: where the value of $\boldsymbol{w}$ is predicted. Hence the $\boldsymbol{w}$ is written as [21]

$$w = [w_o, w_*]^T \begin{cases} w_o = \begin{bmatrix} w(\kappa^*_{o1}) \\ w(\kappa^*_{o2}) \\ \vdots \\ w(\kappa^*_{on_o}) \end{bmatrix} \\ w_* = \begin{bmatrix} w(\kappa^*_{*1}) \\ w(\kappa^*_{*2}) \\ \vdots \\ w(\kappa^*_{*n_*}) \end{bmatrix} \end{cases} \qquad \text{Eq. (19)}$$

As w is a Gaussian process, w_o and w_* are jointly a Gaussian process defined as [21]

$$\begin{pmatrix} w_o \\ w_* \end{pmatrix} \sim N\left(\begin{bmatrix} \mu_o \\ \mu_* \end{bmatrix}, \begin{bmatrix} \Sigma_{oo} & \Sigma_{o*} \\ \Sigma_{*o} & \Sigma_{**} \end{bmatrix} \right) \qquad \text{Eq. (20)}$$

Where μ_p, Σ_{pp}, and, Σ_{pq}, are mean of w_p, variance of w_q and covariance of w_p, w_q respectively which are represented as follows.

$$\mu_o = [m_o(\kappa^*_{o1}), \dots, m_o(\kappa^*_{on_o})] \qquad \text{Eq. (21)}$$

$$\mu_* = [m_*(\kappa^*_{*1}), \dots, m_*(\kappa^*_{*n_*})] \qquad \text{Eq. (22)}$$

$$(\Sigma_{o*})_{i,j} = Cov[w(\kappa^*_{oi}), w(\kappa^*_{*j})] \qquad \text{Eq. (23)}$$

The covariance matrix is described by a kernel function that encodes the smoothness of the objective function. The kernel function used in this study is Squared Exponential Kernel [22], [23]. To estimate the optimum value of the slope parameter without running simulations for each value of κ^*, Bayesian Optimization is used [21].

3.4.2. Bayesian Optimization

The Bayesian Optimization leverages w_o to estimate the values of w_*. The κ^*_{*j} is chosen such that the improvement in estimating the $w(\kappa^*_{*j})$ is maximum. The improvement $I^+(k^*)$ is defined as [21]

$$I^+(k^*) = \begin{cases} w_{min} - w(\kappa^*) \\ 0 \end{cases} \qquad \text{Eq. (24)}$$

$$w_{min} = \min(w_o) \qquad \text{Eq. (25)}$$

As the w_{min} is deterministic and $w(\kappa^*)$ is a Gaussian process, $I^+(\kappa^*)$ follow a normal distribution with mean and variance as $[w_{min} - m(\kappa^*)]$ and $\sigma^2(\kappa^*)$ respectively (see Eq. (26) and Eq. (27)). Further, the best new point is chosen such that the value of acquisition function is maximum. The acquisition function is expressed as given in Eq. (28).

$$m(\kappa^*_j) = m_*(\kappa^*_{*j}) + \Sigma_{jo}\Sigma_{oo}^{-1}(w_o - \mu_o) \qquad \text{Eq. (26)}$$

$$\sigma^2(\kappa^*_j) = Cov[w(\kappa^*_{*j}), w(\kappa^*_{*j})] - \Sigma_{jo}\Sigma_{oo}^{-1}\Sigma_{oj} \qquad \text{Eq. (27)}$$

$$\text{Aquisition Function}(\boldsymbol{\kappa}^*) = EI^+(\boldsymbol{\kappa}^*) = \int_0^\infty I^+ p(I^+(\boldsymbol{\kappa}))dI^+ \qquad \text{Eq. (28)}$$

$$\kappa_i^* = \underset{\underline{\kappa}^* \le \kappa^* \le \overline{\kappa}^*}{argmax}[\text{Aquisition Function}(\boldsymbol{\kappa}^*)] \qquad \text{Eq. (29)}$$

Where $\underline{\kappa}^*$ and $\overline{\kappa}^*$ represent the user-specified limits of the variable $\boldsymbol{\kappa}^*$. In the current study, 3 random initial points are chosen as the noise-free observations, and the next best points are chosen using Bayesian Optimization. The representation of Bayesian Optimization is shown in Fig. 6. For this study, the total number of iterations performed by Bayesian Optimization to estimate the $w(\boldsymbol{\kappa}^*)$ is 50. Further, the optimum point is selected using Eq. (29). This method for estimating the optimum value of parameter for an increasing branch of hysteresis is implemented using the MATLAB function *bayesopt* [16].

(a) Bayesian Optimization suggesting next point

(b) Objective function after running the simulation at the new point
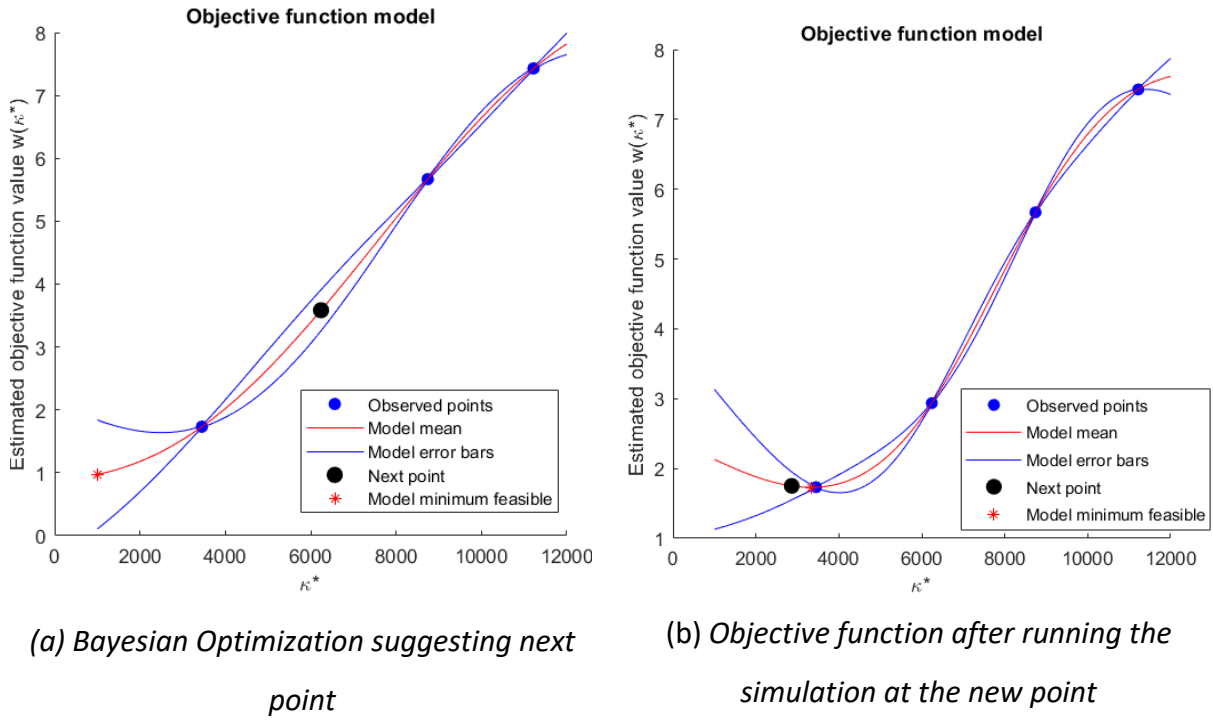
Fig. 6 Working of Bayesian Optimization

Further, the same methodology is repeated for estimating the optimum slope for the positive decreasing $\hat{\kappa}^{**}$, negative increasing $\hat{\kappa}^{***}$, and negative decreasing $\hat{\kappa}^{****}$ branches of the hysteresis curve. The Root Mean Square Error for comparison between the results is defined as

$$RMSE_* = \sqrt{\sum_{i=1}^{i=nd} \frac{\{M(t_i) - m_d(\theta, t_i, \kappa)\}^2}{nd}} \qquad \text{Eq. (30)}$$

3.5. Results

The Dahl model with different slope parameter for each branch of moment-rotation hysteresis is used. Further, the obtained moment-rotation diagram using the Dahl model is compared with the moment-rotation diagram obtained using the Bouc-Wen hysteresis model. Additionally, the hysteretic moment-rotation diagram generated using the Dahl model with different slope parameter is compared with experimental moment-rotation data.

3.5.1. Comparison with data generated using the Bouc-Wen model of hysteresis

From Fig. 7, it is observed that there is a good agreement between the moment-rotation diagram generated using the Dahl model with different slope parameter for each branch and the moment-rotation diagram using the Bouc-Wen hysteresis model. The optimum values of each slope parameter for different branches of hysteresis are reported in Table 4. Further, as seen in Fig. 8, the estimation of the moment in the time domain is accurate with RMSE value of 0.09 KNm.

Table 4 Optimum values of slope parameter in the case of comparison between Bouc-Wen and dahl model hysteresis

Optimum slope parameter	Optimum value
$\hat{\kappa}^*$	4514
$\hat{\kappa}^{**}$	4454
$\hat{\kappa}^{***}$	4351
$\hat{\kappa}^{****}$	4351

(a)

(b)
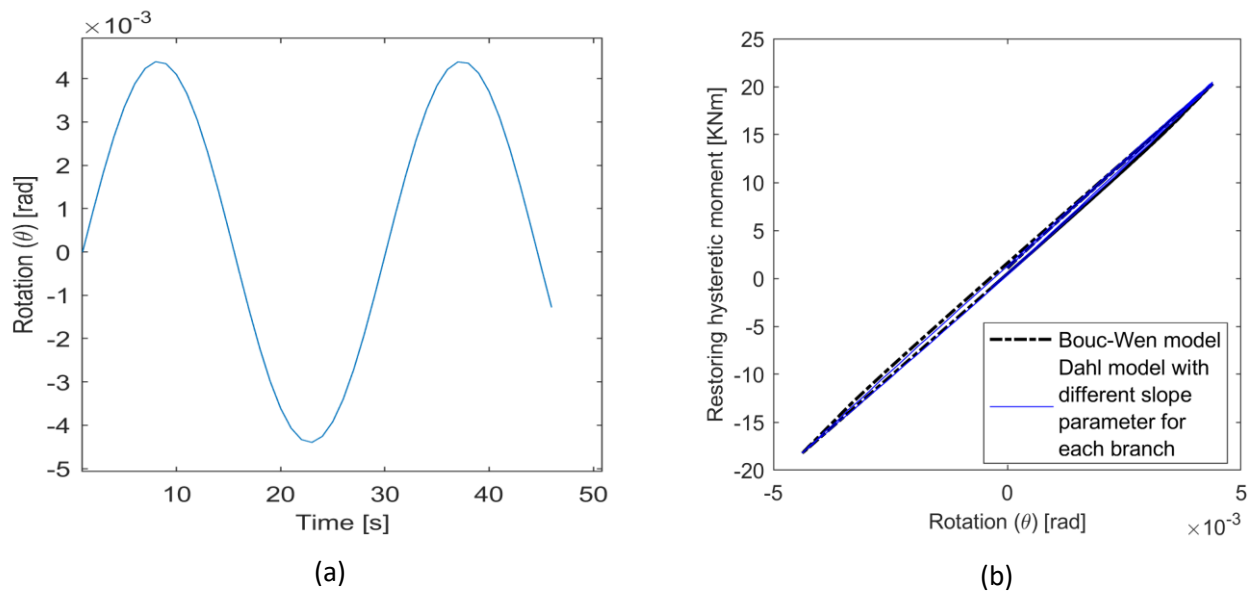
Fig. 7 Rotation of the Bouc-Wen model (a) and comparison between moment-rotation diagram obtained using the Bouc-Wen and the Dahl model with different slope parameter for each branch of hysteresis (b)
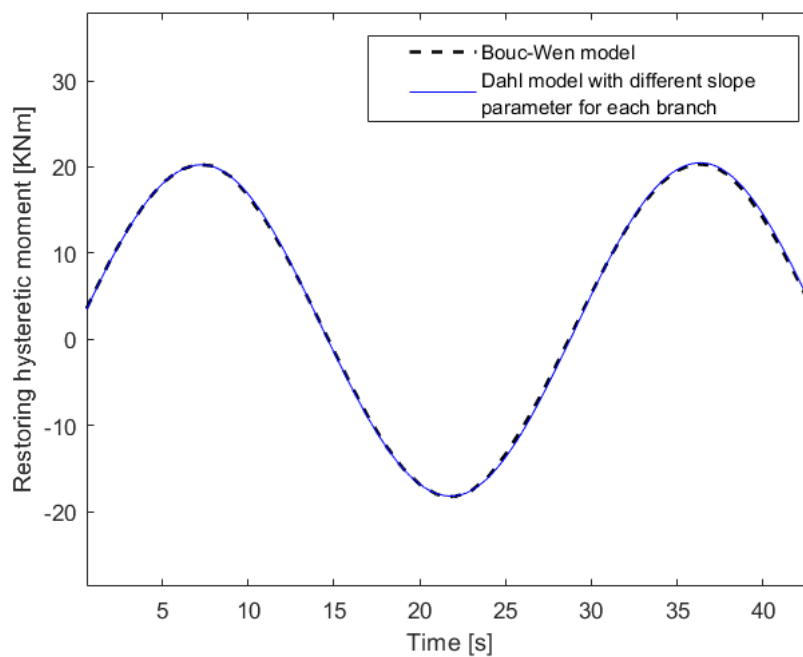
Fig. 8 comparison between moment-rotation diagram obtained using the Bouc-Wen and the Dahl model with different slope parameter for each branch of hysteresis

3.5.2. Comparison with experimental data

Using the data of experimental moment-rotations shown in Fig. 9 and following the methodology mentioned in section 3.2, section 3.3, and section 3.5, the governing equations of the three pinned column base-plate connections are estimated.

Table 5 Values of RMSE and optimum slope parameters for experimental data

	S01	S03	S07
$RMSE_*$ [KNm]	1.05	1.58	1.76
$\hat{\kappa}^*$	4451	6110	50175
$\hat{\kappa}^{**}$	3605	5196	55027
$\hat{\kappa}^{***}$	9510	9501	75010
$\hat{\kappa}^{****}$	8998	8995	80094

As shown in Table 5 and Fig. 9, the obtained results show good accuracy with an acceptable value of RMSE. The obtained moment-rotation diagram using the Dahl model with different slope parameter for each branch of hysteresis exhibit good accuracy. There is a good agreement between the variation of moment in the time domain using the Dahl model and the experimental data as observed in Fig. 10. The values of the optimum slope parameters are stated in Table 5. The error is due to the assumption of a constant slope parameter of the Dahl model for each branch of hysteresis. As the slope parameter is a constant value over one branch of hysteresis, the variation in one branch of the moment-rotation diagram generated using the Dahl model is close to linear. Hence, the local yielding observed in the experimental data though small is not captured.
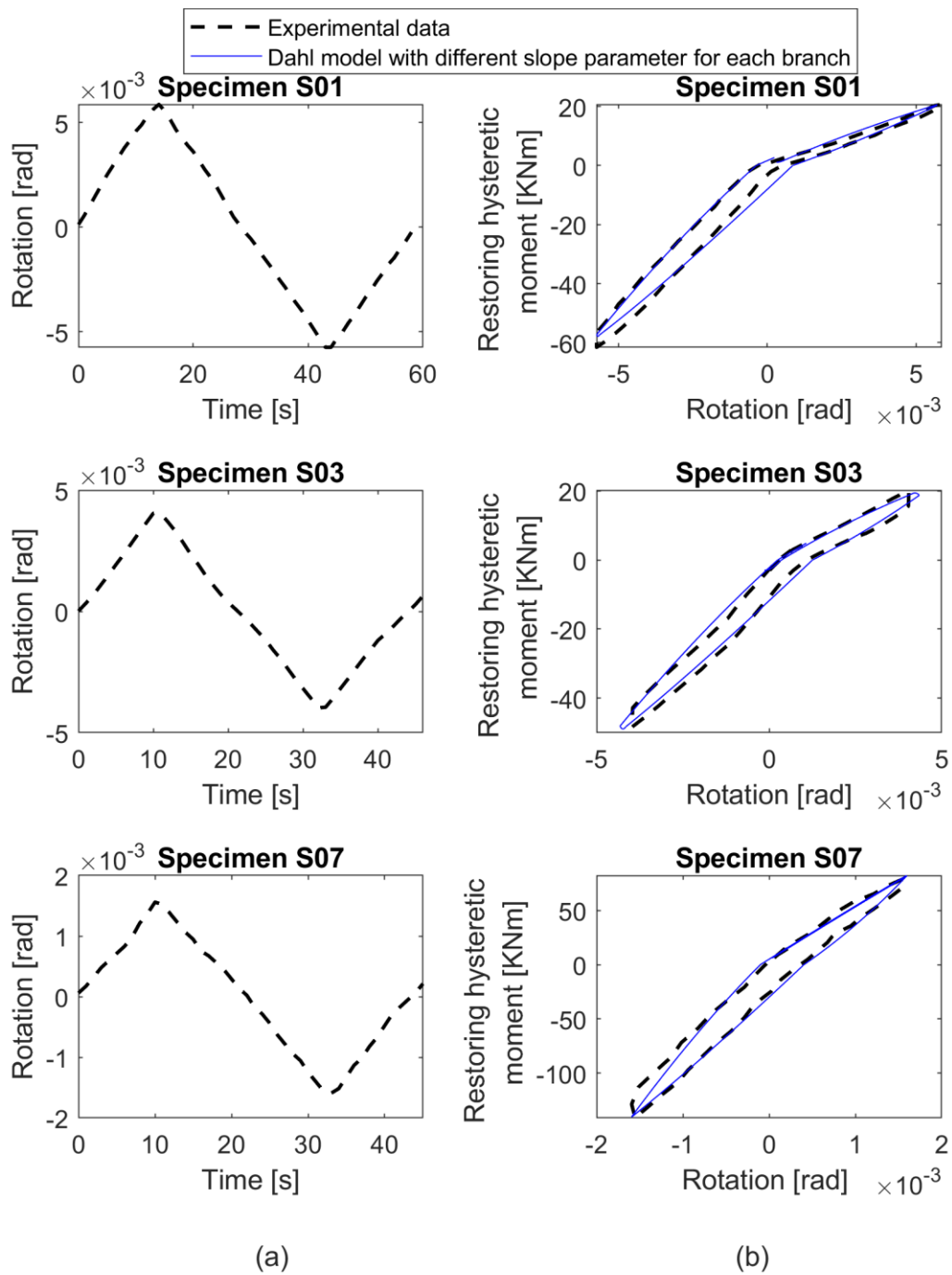
Fig. 9 Data of experimental rotations (a) and restoring hysteretic moment-rotation diagrams of different experimental specimen
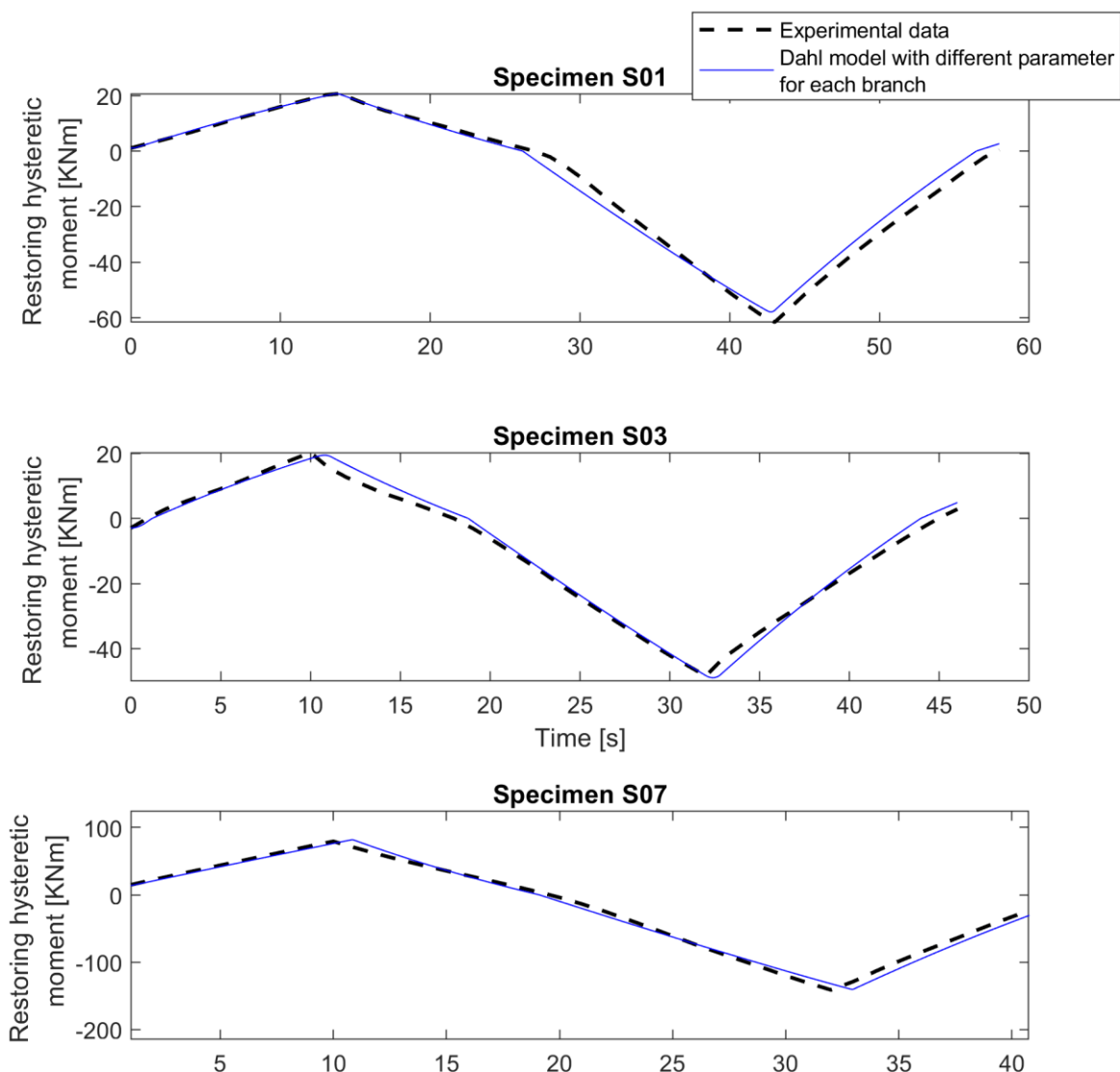
Fig. 10 Comparison between restoring hysteretic moment obtained via experimental investigations and the Dahl model with different slope parameter for each branch of hysteresis

3.6. Conclusions

The methodology for estimating the governing equation of an unsymmetric moment-rotation hysteresis diagram has been proposed. This includes setting different slope parameter in the Dahl model for each branch of the hysteresis diagram. The model is used to estimate the governing equation for the moment-rotation diagram generated using the Bouc-Wen model as well as for the hysteretic moment-rotation diagram of pinned column base-plate connection. The unknown slope parameter of the Dahl model is estimated using Bayesian Optimization.

The main advantage of the proposed approach is, it can be used to identify the governing equation of different types of connection in the elastic region. The identified equations can be used by practicing engineers. The identified equations can be used when the connections have the same geometry and loading conditions. Further, the approach can be used for calculating the loss of energy accurately. As the proposed approach yields a moment-rotation relationship, it can be used for estimating the non-zero rotational stiffness of a connection. The non-zero rotational stiffness will result in increasing the design strength of the structure and hence it can save the material and cost associated with the construction of the building structure. The future work will focus on studying the response of connection under different amplitude of rotation in an elastic region and further in an inelastic region.

Acknowledgement

Bibliography Of Chapter 3

[1]   D. D. Cannon, "Determination of Column Fixity at Column Bases", *AISC,* 1984

[2]   M. Eröz , D. W. White, and R. DesRoches, "Direct Analysis and Design of Steel Frames Accounting for Partially Restrained Column Base Conditions", *Journal of Structural Engineering,* vol. 134, pp. 1508-1517, 2008 https://doi.org/10.1061/(ASCE)0733-9445(2008)134:9(1508)

[3]   T. V. Galambos, "Influence of Partial Base Fixity on Frame Stability", *Journal of the Structural Division*, vol. 86, pp. 85-108, 1960 https://doi.org/10.1061/JSDEAG.0000523

[4]   U. Kim, R. T. Leon, and T. V. Galambos, "Behavior of Steel Joist Girder Structures with Pr Column Bases", *Engineering Journal-American Institute Of Steel Construction*, vol. 44, 2007

[5]   C. Díaz, P. Martí, M. Victoria, and O. M. Querin, "Review on the Modelling of Joint Behaviour in Steel Frames", *Journal of constructional steel research,* vol. 67, pp. 741-758, 2011 https://doi.org/10.1016/j.jcsr.2010.12.014

[6]   Steel Structure Research Committee, "Final Report", Department of Scientific and Industrial Research, London, 1936

[7]   S. R. Lionberger, and W. Weaver, "Dynamic Response of Frames with Nonrigid Connections", *Journal of the Engineering Mechanics Division*, vol.95, pp. 95-114, 1969 https://doi.org/10.1061/JMCEA3.0001087

[8]   K. Romstad, and C. V. Subramanian, "Analysis of Frames with Partial Connection Rigidity", *Journal of the Structural Division*, vol. 96, pp. 2283-2300, 1970 https://doi.org/10.1061/JSDEAG.0002743

[9]   H. Sugimoto, and W. F Chen, "Small End Restraint Effects on Strength of H-Columns", *Journal of the Structural Division*, vol. 108, pp. 661-681, 1982 https://doi.org/10.1061/JSDEAG.0005909

[10]   W. Ramberg, and W. R. Osgood, *Description of Stress-Strain Curves by Three Parameters*, 1943

[11]   F. Kavoura, B. Gencturk, and M. Dawood, "Reversed Cyclic Behavior of Column-to-

Bibliography of Chapter 3

Foundation Connections in Low-Rise Metal Buildings", *Journal of Structural Engineering*, vol. 143, 2017 https://doi.org/10.1061/(ASCE)ST.1943-541X.0001821

[12]   B. Hopkins, T. G. Williams, "The elastic hysteresis of steel", *Proceedings of the Royal Society A*, vol. 87, pp.502-511 1912 https://doi.org/10.1098/rspa.1912.0104

[13]   R. Bouc, "Forced Vibrations of Mechanical Systems with Hysteresis", *Proc. of the Fourth Conference on Nonlinear Oscillations,* 1967

[14]   Y. K. Wen, "Method for Random Vibration of Hysteretic Systems", *Journal of the engineering mechanics division*, vol. 102, pp. 249-263, 1976 https://doi.org/10.1061/JMCEA3.0002106

[15]   P. R. Dahl, "A Solid Friction Model", Aerospace Corp El Segundo, 1968

[16]   M. Pelikan, D. E. Goldberg, and E. Cantú-Paz, "Boa: The Bayesian Optimization Algorithm", *Proceedings of the genetic and evolutionary computation*, vol. 1, pp 525-32, 1999

[17]   J. Song, and A. Der Kiureghian, "Generalized Bouc–Wen Model for Highly Asymmetric Hysteresis", *Journal of engineering mechanics*, vol. 132, pp. 610-618, 2006 https://doi.org/10.1061/(ASCE)0733-9399(2006)132:6(610)

[18]   MATLAB, version 9.9.0.1857802 (R2020b). The Mathworks Inc (2020)

[19]   C. Danielle, "Dahl Friction Modeling", *Thesis,* Massachusetts Institute of Technology, 2004 http://hdl.handle.net/1721.1/32826

[20]   E. Piollet, D. Poquillon, and G. Michon, "Dynamic Hysteresis Modelling of Entangled Cross-Linked Fibres in Shear", *Journal of Sound and Vibration*, vol. 383, pp. 248-264, 2016 https://doi.org/10.1016/j.jsv.2016.06.023

[21]   C. Williams, and C. E. Rasmussen, "*Gaussian Processes for Machine Learning*", MIT press Cambridge, vol. 2, 2006

[22]   "Kernel Function Options", MathWorks, 2023, https://nl.mathworks.com/help/stats/kernel-covariance-function-options.html

[23]   "Select Optimal Machine Learning Hyperparameters Using Bayesian Optimization", MathWorks, https://nl.mathworks.com/help/stats/bayesopt.html

4. Conclusions and Challenges

Civil Engineering structures such as buildings and grandstands experience dissipation of energy due to the Coulomb friction and hysteresis damping in joints. Hence, it is crucial to identify the magnitude of the Coulomb friction force as well as the governing equations representing hysteresis damping in joints. In this research, an effort is made to identify (i) the governing equation of a SDoF dynamic system with the Coulomb friction using the Extended SINDy (ii) the governing equation of the hysteretic moment-rotation by employing the Dahl model with different slope parameter for each branch of hysteresis. This chapter highlights the important findings about the previously stated problem statement in section 1.2 and discusses challenges for future work.

4.1. Conclusions

The existing SINDy algorithm is first used to identify the nonlinear Coulomb friction in a SDoF system subject to external harmonic excitations. The SINDy algorithm fails to identify the correct coefficients of the EOM that denote the system parameters such as mass normalized stiffness, viscous damping, and friction force. Hence, the Extended SINDy algorithm has been proposed which augments the existing SINDy algorithm with the stick and slip temporal constraints. In the Extended SINDy algorithm, the SINDy algorithm is used to identify the correct functional form of the EOM by leveraging the mass-motion data. Further, the stick and slip temporal constraints are employed on the correct functional form of EOM. This is done using constrained optimization.

The Extended SINDy algorithm is first used to identify the synthetic model of a SDoF dynamic system with the nonlinear Coulomb friction. The Extended SINDy yields excellent results by identifying the system parameters like mass normalized stiffness, viscous damping, and the Coulomb friction force more accurately than the SINDy algorithm. Later, the proposed Extended SINDy is employed to identify an experimental SDoF dynamic system with friction contact. The Extended SINDy identifies the system parameters within an acceptable range of RMSE.

To address the second research question, the experimental setup is schematically represented as a rotational SDoF dynamic system with restoring hysteretic moment. Further, the Bouc-Wen model is employed for generating the unsymmetric hysteresis with characteristics resembling the experimental moment-rotation data. Additionally, the hysteresis diagram is divided into four branches based on the values of moments and rotations. Later, the Dahl model with different slope parameter (κ) for each branch of hysteresis is used to identify the governing equation of moment-rotation hysteresis in the time domain. The Bayesian Optimization is employed for estimating the optimum slope parameters of the Dahl model. The governing equations are identified for the hysteresis diagrams generated using the Bouc-Wen model as well as the experimental data of the column base-plate connection. It is assumed that the slope parameter is constant for each branch of hysteresis. Additionally, the order of the Dahl model is assumed to be the same for all branches of the hysteresis diagram. The governing equations are estimated for three different pinned column base-plate connections in an elastic region with a constant amplitude of rotation.

Using the optimum parameters, the Dahl model estimates the moment-rotation diagram with good accuracy. The error between the moment-rotation diagram obtained using the Bouc-Wen model and the Dahl model with different slope parameter is within an acceptable range. The same is observed when the moment-rotation diagram using an experimental setup is compared to the moment-rotation diagram generated using the Dahl model with different slope parameter.

4.2. Challenges

The proposed Extended SINDy algorithm needs to be analyzed when the SDoF dynamic system is subject to random base excitation. The main challenge in the case of random base excitation is the identification of the functional form of EOM in step 2 of the Extended SINDy. When the SDoF dynamic system with the Coulomb friction is excited using harmonic excitation in a continuous regime, SINDy estimates correct coefficients in the EOM. However, this is possible only if the response data has clear distinction between transient as well as steady-state responses. In the case of random excitation, the response

Conclusions and Challenges

of SDoF with Coulomb friction is random and there is no clear distinction between the transient and the steady-state response in the time domain.

Additionally, the proposed Extended SINDy algorithm needs to be analyzed in the case of a MDoF dynamic system with single or multiple friction contacts. Estimating the system parameters in step 3 remains the main challenge in the case of a MDoF dynamic system with the Coulomb friction. The number of parameters (e.g. stiffness, damping and, magnitude of friction force) will increase with the increase in the degrees of freedom. The current methodology in step 3 of the Extended SINDy involves representing the system parameters in x,y,z coordinate system. This is no longer possible when the number of parameters increases. Hence a different optimization approach in step 3 is required to estimate the correct system parameters.

Further, in real Civil Engineering structures, there are different sources of energy dissipation along with the Coulomb friction. Hence it is important to have a knowledge of the functional form of the other dissipative forces to accurately estimate the magnitude of the Coulomb friction force. Furthermore, the measurements collected contain noise which is not always Gaussian. The noise causes errors in numerical differentiation and will affect the performance of the Extended SINDy in step 2 and step 3.

The pinned column base-plate connections are often subject to random excitations which lead to angular rotations with varying amplitude. The current approach considers a constant amplitude of rotations. Hence the current approach considering the Dahl model with different parameter for each branch of hysteresis needs to be extended. In the current methodology, the value of the yield limit (M_c) is constant. Hence the maximum value of restoring hysteretic moment generated by current approach is equal to M_c. In the case of random angular rotations, the maximum value of restoring hysteretic moment varies in time. Therefore, a special attention is required while setting the value of the yield limit (M_c).

When the pinned column base-plate connection is subject to external loading with high amplitude and frequency, the energy dissipation due to heat can be significantly large. Large energy dissipation leads to a wider hysteresis loop. In the case of a wider hysteresis loop, the change in the slope of the branches of the moment-rotation curve is significant as

Conclusions and Challenges

compared to the current experimental case study. The change in the slope of the hysteresis diagram is governed by parameter i. Hence the issue can be solved by setting the correct value of parameter i using Bayesian Optimization.

In Civil Engineering structures, due to fabrication defects, the pinned column base-plate connections experience localised yielding in an elastic region. The current approach is unable to yield an accurate moment-rotation diagram in the case of localised yielding in an elastic region. This is because of the constant value of the slope parameter (κ) for each branch of hysteresis diagram. In the case of localised yielding in an elastic region, the accuracy of the proposed approach can be increased by considering the slope parameter (κ) a function of time.